PERGAMON

International Journal of Solids and Structures 40 (2003) 5723–5752

INTERNATIONAL JOURNAL OF SOLIDS and STRUCTURES

www.elsevier.com/locate/ijsolstr

Periodically supported beam on a visco-elastic layer as a model for dynamic analysis of a high-speed railway track

A.V. Vostroukhov, A.V. Metrikine *

Delft University of Technology, Faculty of Civil Engineering and Geosciences, P.O. Box 5048, 2600 GA Delft, The Netherlands

Received 20 February 2003; received in revised form 20 February 2003

Abstract

This paper presents a theoretical study of the steady state dynamic response of a railway track to a moving train. The model for the railway track consists of two beams on periodically positioned supports that are mounted on a visco-elastic 3D layer. The beams, supports, and layer are employed to model the rails, sleepers and soil, respectively. The axle loading of the train is modeled by point loads that move on the beams. A method is presented that allows to obtain an expression for the steady-state deflection of the rails in a closed form. On the basis of this expression, the vertical deflection of the rails and its dependence on the velocity of the train is analyzed. Critical velocities of the train are determined and the effect of the material damping in the sub-soil and in the pads on the track response at these critical velocities is studied. The effect of the periodic inhomogeneity of the track introduced by the sleepers is studied by comparing the dynamic response of the model at hand to that of a homogenized model, in which the supports are assumed to be not discrete but uniformly distributed along the track. It is shown that the vertical deflection of the rails predicted by these models resemble almost perfectly. The elastic drag experienced by a high-speed train due to excitation of track vibrations is studied. Considering a French TGV as an example, this drag is calculated using both the inhomogeneous and homogenized models of the track and then compared to the rolling and aerodynamic drag.

Keywords: High-speed railway track; 3D dynamic model; Moving load; Elastic drag

1. Introduction

Modern means of railway transportation in Western Europe are being currently developed to further reduce the travelling time for passengers. Cruise velocities of such high-speed trains as French TGV, German ICE, Swedish X-2000, etc. are nowadays in the range of 200–300 km/h and increase continuously. This velocity increase brought a new problem to railway engineering, namely the problem of significant amplification of the train and track vibrations at high train speeds (Kaynia et al., 2000). This amplification

* Corresponding author. Address: Faculty of Civil Engineering, TU Delft, Stevinweg 1, 2928 CN Delft, The Netherlands. Tel.: +31-15-278-4749; fax: +31-15-278-5767.

E-mail address: a.metrikine@citg.tudelft.nl (A.V. Metrikine).

0020-7683/$ - see front matter © 2003 Elsevier Ltd. All rights reserved.
doi:10.1016/S0020-7683(03)00311-1

occurs when a train moves with a velocity that is close to the Rayleigh wave velocity in the sub-soil of a railway track, the latter varying from 150 to 800 km/h, depending on the soil type. Obviously, modern high-speed trains can easily reach the lower threshold. The amplification of the train and track vibrations at high-speed is a threatening phenomenon, which can lead to rapid deterioration of the track structure and may cause derailment of the train. Therefore, railway tracks should be designed so as to prevent such amplification. To enable this design, a dynamic, three-dimensional model for railway tracks is to be developed that takes into account the track–sub-soil interaction.

There exist various formulations of a 3D-prediction-model for train-induced vibrations of the track and surrounding soil. The first analytical 3D modeling of the dynamic response of a railway track was presented by Filippov (1961). He considered the steady-state response of an Euler-Bernoulli beam resting on an elastic half-space to a load moving uniformly over the beam and showed that the vertical deflection of the beam becomes infinite if the load velocity is equal to the Rayleigh wave speed.

Labra (1975) extended the model of Filippov (1961) by accounting for the axial stresses of the rails associated with the temperature extension. He demonstrated that the axial stresses could reduce the critical velocity of the train significantly.

Krylov (1995) proposed a model for prediction of the level of track vibrations generated by a high-speed train. Modeling the ground by elastic half-space, he used an approximate expression for the Green's function of the elastic half-space that takes into account the Rayleigh wave contribution only. In this model, the train loading was represented by a number of point loads moving with a constant velocity and applied to the half-space at the points defined by the sleeper span. The deflection of the rails under applied axle forces was calculated in a quasi-static approximation using a simplistic model for the track: an Euler-Bernoulli beam on Winkler foundation. The author studied the spectrum of ground vibration and showed that the level of vibrations excited by a very fast train, whose velocity exceeds the Rayleigh wave velocity, is huge with respect to that generated by conventional trains (1000–2000 times larger).

Dieterman and Metrikine (1996) investigated a so-called "equivalent stiffness" of a half-space interacting with a beam. They extended the model of Filippov (1961) by considering the sub-seismic, trans-seismic and super-seismic speed ranges of the train. It was shown that the equivalent stiffness is a complex function of the frequency and wavenumber of waves in the beam. These authors also found that there exist two critical velocities of a train as it is modeled by loads of a constant magnitude. The first one equals to the Rayleigh wave speed (as it was found by Filippov, 1961) and the second one is slightly smaller than this speed.

Sheng et al. (1999) studied the ground vibration generated by a harmonic load that moves along a railway track. In this study, the track was represented as a sandwich beam-structure resting on a layered half-space. The investigation showed that the dynamic response of the track depends on the sub-grade structure crucially. Grundmann et al. (1999) drew the same conclusion.

Metrikine and Popp (1999) presented the first analytical study of a 3D, periodically inhomogeneous model for a railway track. The authors considered an Euler–Bernoulli beam mounted to purely elastic half-space through periodically positioned supports. Main attention in this study was paid to evaluation of the equivalent stiffness of the half-space against the sleepers. It was shown that the original 3D problem could be reduced (exactly) to a 1D model, by replacing the half-space by a system of identical equivalent springs placed under the sleepers, the stiffness of these springs being a complex function of the frequency and phase shift between vibrations of neighboring supports. The authors showed that the Rayleigh wave speed plays a crucial role in dynamics of the model. However, no computations on the beam response to the load were presented in the paper.

Metrikine et al. (2001) enlightened a problem of the energy loss of the train's engine on excitation of vibrations of the track and soil. The authors explored the question on whether the generation of ground vibration might lead to perceptible increase of the energy consumption. In this study, an enhanced model of Filippov (1961) was employed. The analysis was carried out by means of introduction of the term "elastic drag", which is a measure for the energy loss that a moving train experiences due to excitation of ground

vibration. The authors showed that although the elastic drag grows significantly as the train approaches the Rayleigh wave velocity, it is very small with respect to the aerodynamic drag.

Thanks to rapid development of computational technologies in the 1990s it became possible to use the boundary-element method (BEM) and hybrid boundary-finite-element methods (BEM-FEM) for investigation of ground vibration and dynamic behavior of the railway track. Recent developments of this approach can be exemplified by papers of Kaynia et al. (2000) and Van den Broeck et al. (2002), which are distinguished from other publications by comprehensive comparison of theoretical results to in situ measurements.

Kaynia et al. (2000) presented results of measurements carried out by Swedish Geotechnical Institute at a site of the West Coast Line between Göteborg and Malmö where the soil is extremely soft. The test runs were performed using a Sweden X-2000 passenger train composed of one locomotive and four cars. The tests showed that significant amplification occurs of vibration of the railway track at velocities close to the Rayleigh wave speed, which turned out to be very low in this part of the track—about 40 m/s. The authors proposed a method for simulation of ground vibration from high-speed train based on the Kausel-Roësset Green's function (1981). They modeled the ground as a layered visco-elastic half-space and the track as an Euler–Bernoulli beam. Forces, uniformly moving at fixed distances from each other were employed to model the loading by the train. The authors found a very good agreement between the measurements and their computational simulations. On the basis of the developed model they studied the effect of stiffer embankment (beam) and showed that increasing of the embankment's bending stiffness results in substantial reduction of the vibration level.

Van den Broeck et al. (2002) developed a model of the railway track accounting for discretely positioned sleepers, the soil stratification, the wheel/rail interaction and the unevenness of the rails. Although, this model allows to study both the ground vibration and the train–track interaction, main attention in this paper was paid to spectral analysis of the ground vibration and demonstration of the crucial role of the soil stratification.

The present study is a development of the analytical approach to the problem that was proposed by Metrikine and Popp (1999). This approach uses approximate boundary conditions at the sleeper–soil interface in order to obtain a closed-form, steady-state solution of the problem. This solution allows to calculate the dynamic response of the railway track relatively fast, as compared to FEM and FEM-BEM methods.

In the present paper, the method proposed by Metrikine and Popp (1999) is improved so that it can account for stratified, visco-elastic soils. The other original element of this paper is that the tangential stresses at the sleeper–soil interface are taken into account (in approximate manner). Along with improvement of the method and enhancement of the model, this paper focuses on a number of issues, which did not receive enough attention in the past. These issues are

1. Effect of the material damping in the soil and the damping in the pads on the dynamic response of the track to a train that moves with a critical velocity;
2. Effect of longitudinal inhomogeneity of the track (introduced by the sleepers) on its dynamic response to a moving train. This effect is studied by comparing the response of an inhomogeneous model for the track to that of a homogenized one, in which the sleepers are assumed to be uniformly and continuously distributed along the track;
3. The elastic drag that trains experience due to excitation of ground vibration and those of the rails. As shown by Metrikine et al. (2001), this drag can grow significantly as a train moves with a high-speed. In this paper, it is studied whether the inhomogeneity of the track can influence the drag perceptibly.

In the present study, a model is employed that consists of two Euler–Bernoulli beams on periodically positioned supports and a visco-elastic layer. The beams, supports, and layer are used to model the rails,

sleepers and soil, respectively. Point loads that move on the beams model the axle loading of the train. The loads are assumed vertical and imposed by the weight of the train only (the magnitude of the loads is time-independent).

The paper is structured as follows. In Section 2, a mathematical statement of the problem is presented along with assumptions with which this model is valid. Then, applying the integral Fourier transform transition to the frequency–wavenumber domain is performed. In Section 3, the concept of the equivalent dynamic stiffness of the ground at the interfaces with the sleepers (Metrikine and Popp, 1999) is elaborated. Using this stiffness, the original 3D model is reduced exactly (in the frequency domain) to an equivalent 1D model and the steady-state response of the structure is studied. Main attention is paid to the vertical deflection of the rails and its dependence on the load velocity. Critical velocities are determined and the effect of parameters of the model on the track response at these critical velocities is studied. Obtained results are compared to those that follow from a homogenized model of the track, in which the sleepers are assumed to be uniformly and continuously distributed along the rails. In Section 4, elastic drag experienced by a high-speed train due to excitation of track vibrations is studied. First, the drag experienced by a single axle is calculated and compared to that obtained by Metrikine et al. (2001), the latter having been calculated by using a homogenized model. Second, to study the effect of the bogie wheelbase, the drag is studied for two axles. Finally, the total elastic drag that is experienced by a French TGV is calculated and compared to the results of Metrikine et al. (2001) and to the rolling and aerodynamic drag.

2. Model

2.1. Basic assumptions and mathematical statement of the problem in the time domain

We consider the steady-state vibrations of a railway track, whose model is presented in Fig. 1. This model is composed of two beams on periodically positioned supports (sleepers) and a visco-elastic layer of depth H that underlies the supports. The structure is excited by eight point loads of constant amplitude P that move along the beams with constant speed V. These loads account for the weight of a train's wagon disregarding dynamic variation of the contact force.

To model the contact between the sleepers and the layer, it is assumed that the surface tractions are uniformly distributed over the contact area. This assumption is approximate and valid only for those processes in the layer, whose spatial scale is much larger than the maximum dimension of the contact area. Thus, with this assumption we may consider low-frequency vibrations of the railway track only, the low-frequency implying that the waves in the soil, which correspond to these vibrations, are long as compared to

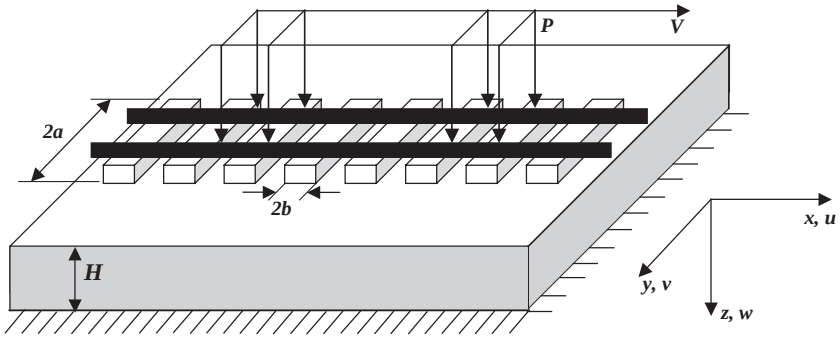

Fig. 1. Model: a visco-elastic layer overlaid by two beams on periodically positioned supports.

the sleepers. This is precisely the frequency band that is relevant for the present study. Indeed, in this paper, we model the train as a system of constant vertical loads. In this case, the spectrum of dynamic response of the railway track is located (up to 95%) in the low-frequency range so that the assumption under discussion is applicable.

The compatibility condition between the sleepers and the surface of the layer can be simplified in the low-frequency band as well. In this band, having waves in the layer much longer than the sleepers, it is sufficient to require that the displacements of the sleeper are equal (or proportional) to those of the surface of the layer in the center of the contact area.

As shown by Metrikine and Dieterman (1997), with the above-discussed assumptions, the lateral motion of a sleeper is uncoupled from its longitudinal and vertical motion. Therefore, under the vertical loading, the lateral surface traction τ_{zy} under the sleepers can be disregarded.

The model for the sleeper–layer contact in the vertical plane is schematized in Fig. 2.

We assume that the vertical displacement of each sleeper is equal to that of the layer (in the middle point of the contact area). The horizontal displacement of the sleeper is disregarded but the layer is allowed to move with respect to the sleeper, subjected to elastic reaction of a spring K. This spring is assumed to be uniformly distributed over the contact area and its reaction to be proportional to the x-displacement of the layer under the center point of the contact area. The spring K is introduced into the model to account for possible longitudinal elasticity (not necessarily equal to the vertical one) of the ballast, which is not explicitly accounted for in the model.

The further assumptions adopted are:

- the beams are infinitely long and modeled in accordance with the Euler–Bernoulli theory (sufficient in the low-frequency range);
- the sleepers are rigid;
- the pads that connect the sleepers and the rails are modeled as spring-dashpot elements;
- the contact area between each support and the layer is a rectangle of the size $2a \times 2b$;
- no break of contact between the sleepers and the layer is permitted;
- the layer is considered as visco-elastic in accordance with the Kelvin–Voigt model and is fixed at its bottom.

Finally, we note that because of the symmetry of the loading with respect to the centerline $y = 0$ of the track, the sleepers will move vertically and the rails will vibrate identically. Because of the latter, in the mathematical statement of the problem, only one equation of motion for the beam is presented.

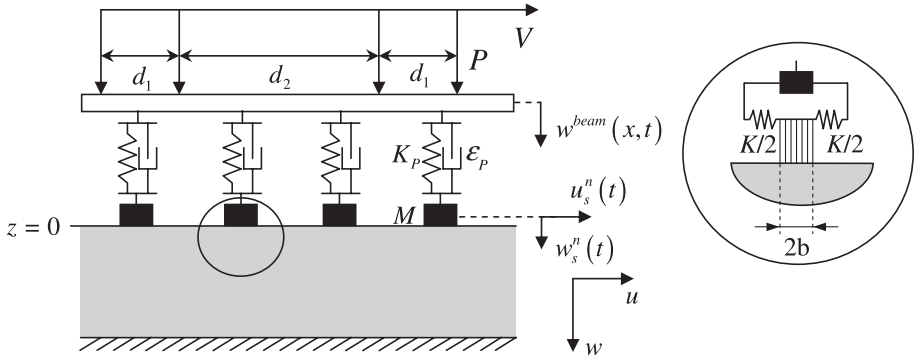

Fig. 2. Vertical cross-section $y = 0$ and magnified "sleepers-layer" interface showing the model for interaction in the x-direction.

With all aforementioned assumptions, the governing equations of motion can be written as follows.

The equation of motion for the layer

$$\hat{\mu}\Delta\boldsymbol{u} + (\hat{\lambda} + \hat{\mu})\nabla(\nabla \cdot \boldsymbol{u}) = \rho\partial_{tt}\boldsymbol{u}, \tag{1}$$

where $\boldsymbol{u}(x,y,z,t) = (u(x,y,z,t), v(x,y,z,t), w(x,y,z,t))$ is the displacement, ρ is mass density, $\hat{\lambda} = \lambda + \lambda^*\partial/\partial t$ and $\hat{\mu} = \mu + \mu^*\partial/\partial t$ are operators that are used instead of Lamé's constants λ and μ to describe the layer according to the Voigt phenomenological model.

The boundary conditions at the surface $z = 0$ of the layer

$$\begin{aligned}
\sigma_{zz}(x,y,0,t) &= \frac{H(a-|y|)}{4ab}\sum_{n=-\infty}^{\infty}[M\partial_{tt}w_{\mathrm{s}}^{n}(t) + 2(K_{\mathrm{p}} + \varepsilon_{\mathrm{p}}\partial_t)(w_{\mathrm{s}}^{n}(t) - w^{\mathrm{beam}}(nd,t))]H(b-|x-nd|),\\
\tau_{zx}(x,y,0,t) &= \frac{H(a-|y|)}{4ab}\sum_{n=-\infty}^{\infty}Ku(nd,0,0,t)H(b-|x-nd|), \quad \tau_{zy}(x,y,0,t) = 0,
\end{aligned} \tag{2}$$

where $\sigma_{zz}(x,y,0,t)$, $\tau_{zx}(x,y,0,t)$ and $\tau_{zy}(x,y,0,t)$ are the vertical, longitudinal and lateral tractions at $z = 0$, $w^{\mathrm{beam}}(x,t)$ is the vertical displacement of the beam, $w_{\mathrm{s}}^{n}(t)$ is the vertical displacement of the sleeper number n, K_{p} and ε_{p} are the stiffness and damping coefficient of a pad, respectively, M is the mass of a sleeper, K is the stiffness per unit length of the longitudinal springs at the "sleeper–layer" interface, $H(\cdots)$ is the Heaviside step function.

The boundary conditions at the bottom $z = H$ of the layer

$$\boldsymbol{u}(x,y,H,t) = 0 \tag{3}$$

The compatibility condition for the vertical motion of the sleepers and layer

$$w_{\mathrm{s}}^{n}(t) = w(nd,0,0,t) \tag{4}$$

The equation of motion for one of the beams

$$\begin{aligned}
\rho_{\mathrm{beam}}S\partial_{tt}w^{\mathrm{beam}} + E_{\mathrm{beam}}I\partial_{xxxx}w^{\mathrm{beam}} = {} & \sum_{n=-\infty}^{\infty}[(K_{\mathrm{p}} + \varepsilon_{\mathrm{p}}\partial_t)(w_{\mathrm{s}}^{n}(t) - w^{\mathrm{beam}}(nd,t))]\delta(x-nd) + P(\delta(x-Vt)\\
& + \delta(x-Vt+d_1) + \delta(x-Vt+d_1+d_2) + \delta(x-Vt+2d_1+d_2)),
\end{aligned} \tag{5}$$

where $\rho_{\mathrm{beam}}S$ and $E_{\mathrm{beam}}I$ are the mass per unit length and the bending stiffness of the beam, respectively, d_1 and d_2 are the distances between the loads as depicted in Fig. 2, and $\delta(\cdots)$ is the Dirac delta function.

2.2. Transformation into the frequency–wavenumber domain

To solve the system of governing equations (1)–(5), it is convenient to use the Helmholtz decomposition of the displacement vector $\boldsymbol{u}$:

$$\boldsymbol{u} = \nabla\varphi + \nabla \times \boldsymbol{\psi}, \quad \nabla \cdot \boldsymbol{\psi} = 0. \tag{6}$$

In terms of the potentials φ and $\boldsymbol{\psi} = \{\psi_x, \psi_y, \psi_z\}$, the equations of motion for the layer read (Achenbach, 1973):

$$\hat{c}_{\mathrm{L}}^2\Delta\varphi = \partial_{tt}\varphi, \quad \hat{c}_{\mathrm{T}}^2\Delta\boldsymbol{\psi} = \partial_{tt}\boldsymbol{\psi}, \quad \nabla \cdot \boldsymbol{\psi} = 0, \tag{7}$$

with $\hat{c}_{\mathrm{L}}^2 = (\hat{\lambda} + 2\hat{\mu})/\rho, \hat{c}_{\mathrm{T}}^2 = \hat{\mu}/\rho$. Expressions for the displacement vector $\boldsymbol{u}$ and stresses σ_{zz}, τ_{zx}, τ_{zy} in terms of these potentials are given in Appendix A.

To find the steady-state solution to the problem at hand, we apply integral Fourier transforms with respect to the time and horizontal co-ordinates. The signs of these transforms are defined as

$$f_{\omega,k_1,k_2} = \int_{-\infty}^{\infty}\int_{-\infty}^{\infty}\int_{-\infty}^{\infty} f(x,y,t)\exp(\mathrm{i}\omega t - \mathrm{i}k_1 x - \mathrm{i}k_2 y)\,\mathrm{d}x\,\mathrm{d}y\,\mathrm{d}t. \tag{8}$$

Throughout the paper, transformed quantities are given the subscripts ω, k_1 and k_2 to show that the transformation was applied with respect to the time, x-coordinate and y-coordinate, respectively.

Application of the Fourier transforms to the system of equations (2)–(5), (7), gives the system of equations in the frequency–wavenumber domain that is presented below.

The equation of motion for the layer (from Eq. (7))

$$\partial_{zz}\varphi_{\omega,k_1,k_2} + R_{\mathrm{L}}^2\varphi_{\omega,k_1,k_2} = 0, \quad \partial_{zz}\boldsymbol{\psi}_{\omega,k_1,k_2} + R_{\mathrm{T}}^2\boldsymbol{\psi}_{\omega,k_1,k_2} = 0, \tag{9}$$

$$\mathrm{i}k_1(\psi_x)_{\omega,k_1,k_2} + \mathrm{i}k_2(\psi_y)_{\omega,k_1,k_2} + \partial_z(\psi_z)_{\omega,k_1,k_2} = 0, \tag{10}$$

where $R_{\mathrm{L,T}} = \sqrt{k_1^2 + k_2^2 - \omega^2/\tilde{c}_{\mathrm{L,T}}^2}$, $\tilde{c}_{\mathrm{L}}^2 = c_{\mathrm{L}}^2 - \mathrm{i}\omega(\lambda^* + 2\mu^*)/\rho$, $\tilde{c}_{\mathrm{T}}^2 = c_{\mathrm{T}}^2 - \mathrm{i}\omega\mu^*/\rho$, $c_{\mathrm{L}} = \sqrt{(\lambda+2\mu)/\rho}$ is the propagation velocity of the dilatational waves (P-waves), $c_{\mathrm{T}} = \sqrt{\mu/\rho}$ is the propagation velocity of the shear waves (S-waves).

The boundary conditions at the surface $z = 0$ of the layer (from Eq. (2), using Eqs. (A.2)–(A.4)):

$$\begin{aligned}
&\tilde{\lambda}(\partial_{zz} - k_1^2 - k_2^2)\varphi_{\omega,k_1,k_2} + 2\tilde{\mu}(\partial_{zz}\varphi_{\omega,k_1,k_2} + \partial_z(\mathrm{i}k_1(\psi_y)_{\omega,k_1,k_2} - \mathrm{i}k_2(\psi_x)_{\omega,k_1,k_2})) = \frac{\sin k_1 b}{k_1 b}\frac{\sin k_2 a}{k_2 a}\\
&\quad\times\sum_{n=-\infty}^{\infty}[-M\omega^2(w_{\mathrm{s}}^n)_\omega + 2(K_{\mathrm{p}} - \mathrm{i}\varepsilon_{\mathrm{p}}\omega)(w_\omega(nd,0,0,\omega) - w_\omega^{\mathrm{beam}}(nd,\omega))]\exp(-\mathrm{i}k_1 nd),\\
&2\mathrm{i}k_1\partial_z\varphi_{\omega,k_1,k_2} + \partial_z(\mathrm{i}k_2(\psi_z)_{\omega,k_1,k_2} - \partial_z(\psi_y)_{\omega,k_1,k_2}) + \mathrm{i}k_1(\mathrm{i}k_1(\psi_y)_{\omega,k_1,k_2} - \mathrm{i}k_2(\psi_x)_{\omega,k_1,k_2})\\
&\quad = \frac{1}{\tilde{\mu}}\frac{\sin k_1 b}{k_1 b}\frac{\sin k_2 a}{k_2 a}\sum_{n=-\infty}^{\infty} Ku_\omega(nd,0,0,\omega)\exp(-\mathrm{i}k_1 nd),\\
&2\mathrm{i}k_2\partial_z\varphi_{\omega,k_1,k_2} - \partial_z(\mathrm{i}k_1(\psi_z)_{\omega,k_1,k_2} - \partial_z(\psi_x)_{\omega,k_1,k_2}) + \mathrm{i}k_2(\mathrm{i}k_1(\psi_y)_{\omega,k_1,k_2} - \mathrm{i}k_2(\psi_x)_{\omega,k_1,k_2}) = 0,
\end{aligned} \tag{11}$$

where $\tilde{\lambda} = \lambda - \mathrm{i}\omega\lambda^*$, $\tilde{\mu} = \mu - \mathrm{i}\omega\mu^*$.

The boundary conditions at the bottom $z = H$ of the layer (from Eq. (3), using Eq. (A.1)):

$$\begin{aligned}
&\mathrm{i}k_1\varphi_{\omega,k_1,k_2} + \mathrm{i}k_2(\psi_z)_{\omega,k_1,k_2} - \partial_z(\psi_y)_{\omega,k_1,k_2} = 0,\\
&\mathrm{i}k_2\varphi_{\omega,k_1,k_2} - \mathrm{i}k_1(\psi_z)_{\omega,k_1,k_2} + \partial_z(\psi_x)_{\omega,k_1,k_2} = 0,\\
&\partial_z\varphi_{\omega,k_1,k_2} + \mathrm{i}k_1(\psi_y)_{\omega,k_1,k_2} - \mathrm{i}k_2(\psi_x)_{\omega,k_1,k_2} = 0.
\end{aligned} \tag{12}$$

The compatibility condition for the vertical motion of the sleepers and layer (from Eq. (4)):

$$(w_{\mathrm{s}}^n)_\omega = w_\omega(nd,0,0,\omega). \tag{13}$$

The equation of motion for one of the beams (from Eq. (5), using Eq. (13))

$$\begin{aligned}
(-\rho_{\mathrm{beam}}S\omega^2 + E_{\mathrm{beam}}Ik_1^4)w_{\omega,k_1}^{\mathrm{beam}} = {}& 2\pi P\delta(\omega - k_1 V)\left(1 + \exp\left(\mathrm{i}d_1\frac{\omega}{V}\right) + \exp\left(\mathrm{i}(d_1+d_2)\frac{\omega}{V}\right)\right.\\
&\left. + \exp\left(\mathrm{i}(2d_1+d_2)\frac{\omega}{V}\right)\right) + \sum_{n=-\infty}^{\infty}(K_{\mathrm{p}} - \mathrm{i}\omega\varepsilon_{\mathrm{p}})(w_\omega(nd,0,0,\omega)\\
&- w_\omega^{\mathrm{beam}}(nd,\omega))\exp(-\mathrm{i}k_1 nd).
\end{aligned} \tag{14}$$

In the next section, the system of Eqs. (9)–(14) will be evaluated using a method presented by Metrikine and Popp (1999). In accordance with this method, reaction of the layer against a sleeper can be replaced (in the frequency domain) by an equivalent spring whose dynamic stiffness is a complex-valued function of frequency and wavelength of waves in the beam. In the steady-state regime imposed by a uniformly moving

load, all equivalent springs (there are infinitely many of them, one for each sleeper) have the same stiffness, which becomes a function of frequency and a phase shift between vibrations of neighboring supports. This phase shift is the same for every pair of neighboring supports and depends on the frequency of vibrations, velocity of the load and the sleeper distance.

3. Steady-state response of the structure

3.1. Dynamic stiffness of the layer

The system of Eqs. (9)–(14) is evaluated on the basis of the general solution of Eq. (9). This solution reads

$$\begin{aligned} &\varphi_{\omega,k_1,k_2} = A_1 e^{R_L z} + A_2 e^{-R_L z}, \quad (\psi_x)_{\omega,k_1,k_2} = A_3 e^{R_T z} + A_4 e^{-R_T z}, \\ &(\psi_y)_{\omega,k_1,k_2} = A_5 e^{R_T z} + A_6 e^{-R_T z}, \quad (\psi_z)_{\omega,k_1,k_2} = A_7 e^{R_T z} + A_8 e^{-R_T z}. \end{aligned} \tag{15}$$

Substituting solution (15) into Eq. (10) and boundary conditions Eqs. (11) and (12), a system of eight algebraic equations with respect to A_i, $i = 1, 8$ can be obtained, the matrix form of which is given as

$$[\boldsymbol{C}]\boldsymbol{A} = \boldsymbol{F}, \tag{16}$$

with matrix $[\boldsymbol{C}]$ and vector $\boldsymbol{F}$ defined in Appendix B.

The system of algebraic Eq. (16) can be solved readily to give analytical expressions for A_i, $i = 1, 8$. Subsequently substituting these expressions into Eq. (15) and transformed (into the frequency–wavenumber domain) Eq. (A.1) the following expressions for the Fourier displacements of the surface of the layer in the x- and z-directions can be obtained

$$u_{\omega,k_1,k_2}(k_1,k_2,0,\omega) = a_{11}F_1 + a_{13}F_3, \quad w_{\omega,k_1,k_2}(k_1,k_2,0,\omega) = a_{31}F_1 + a_{33}F_3, \tag{17}$$

with a_{11}, a_{13}, a_{31}, a_{33}, F_1 and F_3 defined in Appendix B.

Application of the inverse Fourier transforms over the wavenumbers k_1 and k_2 to Eq. (17), followed by substitutions $x = md$ and $y = 0$, yields

$$\begin{aligned} u_\omega(md,0,0,\omega) &= \frac{1}{4\pi^2}\int_{-\infty}^{\infty}\int_{-\infty}^{\infty}(a_{11}F_1 + a_{13}F_3)e^{ik_1 md}\,dk_1\,dk_2, \\ w_\omega(md,0,0,\omega) &= \frac{1}{4\pi^2}\int_{-\infty}^{\infty}\int_{-\infty}^{\infty}(a_{31}F_1 + a_{33}F_3)e^{ik_1 md}\,dk_1\,dk_2. \end{aligned} \tag{18}$$

Eqs. (18) establish the relationship between the displacements $u_\omega(md,0,0,\omega)$ and $w_\omega(md,0,0,\omega)$ of the layer under the midpoints of the sleepers and the vertical displacement $w_\omega^{\text{beam}}(nd,\omega)$ of the beam in the supported points (the latter displacement contains in F_3, see Eq. (B.3)).

To find the steady-state response of the structure, we have to couple Eq. (18) with the equation of motion for the beam (14). Solving the latter with respect to $w_{\omega,k_1}^{\text{beam}}$, applying to the result the inverse Fourier transform over k_1 and using the compatibility condition (13), we obtain

$$\begin{aligned} w_\omega^{\text{beam}}(md,\omega) = {} & \frac{1}{2\pi}\int_{-\infty}^{\infty}\frac{2\pi P\delta(\omega - k_1 V)e^{ik_1 md}\,dk_1}{E_{\text{beam}}Ik_1^4 - \rho_{\text{beam}}S\omega^2}\left(1 + e^{id_1(\omega/V)} + e^{i(d_1+d_2)(\omega/V)} + e^{i(2d_1+d_2)(\omega/V)}\right) \\ & + \frac{1}{2\pi}\sum_{n=-\infty}^{\infty}\left[(K_p - i\omega\varepsilon_p)(w_\omega(nd,0,0,\omega) - w_\omega^{\text{beam}}(nd,\omega))\right]\int_{-\infty}^{\infty}\frac{e^{ik_1 md}e^{-ik_1 nd}\,dk_1}{E_{\text{beam}}Ik_1^4 - \rho_{\text{beam}}S\omega^2}. \end{aligned} \tag{19}$$

The first integral in Eq. (19) can be evaluated analytically to give

$$w_{\omega}^{\text{beam}}(md,\omega) = \frac{PV^3 e^{i(\omega/V)md}}{E_{\text{beam}}I\omega^4 - \rho_{\text{beam}}S\omega^2V^4}\left(1 + e^{id_1(\omega/V)} + e^{i(d_1+d_2)(\omega/V)} + e^{i(2d_1+d_2)(\omega/V)}\right) + \frac{1}{2\pi}\sum_{n=-\infty}^{\infty}\left[(K_p - i\omega\varepsilon_p)(w_{\omega}(nd,0,0,\omega) - w_{\omega}^{\text{beam}}(nd,\omega))\right]\int_{-\infty}^{\infty}\frac{e^{ik_1md}e^{-ik_1nd}\,dk_1}{E_{\text{beam}}Ik_1^4 - \rho_{\text{beam}}S\omega^2}. \tag{20}$$

The first term on the right-hand side of Eq. (20) is the "loading term", which determines the spatial variation of the steady-state response in the frequency domain. All displacements in the frequency domain must comply with this term e.g. expressions for all displacements must be proportional to $\exp(i\omega md/V)$. Thus, to find the steady-state response of the structure, we have to search for the solution of Eqs. (18) and (20) in the form

$$\begin{aligned} w_{\omega}^{\text{beam}}(md,\omega) &= C_0(\omega)\exp(i\omega md/V),\\ w_{\omega}(md,0,0,\omega) &= C(\omega)\exp(i\omega md/V),\\ u_{\omega}(md,0,0,\omega) &= A(\omega)\exp(i\omega md/V), \end{aligned} \tag{21}$$

where $C_0(\omega)$, $C(\omega)$ and $A(\omega)$ are unknown functions of frequency.

Substituting Eq. (21) into Eq. (20), and employing Eq. (18), we obtain the following system of algebraic equations with respect to $C_0(\omega)$, $C(\omega)$ and $A(\omega)$:

$$\begin{aligned} A &= KJ_{11}A + J_{13}(C_0(K_p - i\omega\varepsilon_p) + (-M\omega^2 + K_p - i\omega\varepsilon_p)C),\\ C &= KJ_{31}A + J_{33}(C_0(K_p - i\omega\varepsilon_p) + (-M\omega^2 + K_p - i\omega\varepsilon_p)C), \end{aligned} \tag{22}$$

with

$$J_{kj} = \frac{1}{4\pi^2\tilde{\mu}}\int_{-\infty}^{\infty}\int_{-\infty}^{\infty}a_{kj}\frac{\sin k_1b}{k_1b}\frac{\sin k_2a}{k_2a}\sum_{n=-\infty}^{\infty}\exp(ik_1d(m-n) - iq(m-n))\,dk_1\,dk_2. \tag{23}$$

Parameter q in Eq. (23) is given as

$$q = \frac{\omega}{V}d \tag{24}$$

and represents the phase shift between vibrations of neighboring sleepers.

In Eq. (22), A and C are the amplitudes of the horizontal (in the x-direction) and vertical vibrations of the layer surface under the midpoint of a sleeper, respectively, whereas C_0 is the amplitude of the vertical vibrations of the beam in the point that is supported by this sleeper. These equations can be rewritten in the following matrix form

$$\begin{bmatrix} KJ_{11} - 1 & J_{13}(-M\omega^2 + K_p - i\omega\varepsilon_p)\\ KJ_{31} & J_{33}(-M\omega^2 + K_p - i\omega\varepsilon_p) - 1 \end{bmatrix}\begin{bmatrix} A\\ C \end{bmatrix} = -C_0(K_p - i\omega\varepsilon_p)\begin{bmatrix} J_{13}\\ J_{33} \end{bmatrix}. \tag{25}$$

Now, employing the conception of the equivalent dynamic stiffness proposed by Dieterman and Metrikine (1996), we introduce a complex stiffness matrix $\boldsymbol{\chi}_{\text{l-s}}$ that describes the dynamic stiffness of the layer at the contact point with a sleeper. The inverse to this matrix (the compliance matrix) is defined as

$$\boldsymbol{\chi}_{\text{l-s}}^{-1} = \begin{bmatrix} -J_{11} & -J_{13}\\ -J_{31} & -J_{33} \end{bmatrix} \tag{26}$$

and depends on the angular frequency ω and the phase shift q between vibrations of neighboring sleepers. Employing the equivalent stiffness matrix $\boldsymbol{\chi}_{\text{l-s}}$, Eq. (25) can be rewritten in the following, more comprehensible form

$$(\boldsymbol{K}+\boldsymbol{K}_{\text{ps}}+\boldsymbol{M}_{\text{ps}}+\boldsymbol{C}_{\text{ps}}+\boldsymbol{\chi}_{\text{l-s}})\begin{bmatrix}A\\C\end{bmatrix}=(\boldsymbol{K}_{\text{ps}}+\boldsymbol{C}_{\text{ps}})\begin{bmatrix}0\\C_0\end{bmatrix} \tag{27}$$

with $\boldsymbol{K}$ the stiffness matrix of the interface between the sleepers and the layer surface, $\boldsymbol{M}_{\text{ps}}$, $\boldsymbol{K}_{\text{ps}}$ and $\boldsymbol{C}_{\text{ps}}$ the mass, stiffness and damping matrices of the sleeper-pad system. These matrices in the case at hand are given as

$$\boldsymbol{K}=\begin{bmatrix}\boldsymbol{K}&0\\0&0\end{bmatrix},\quad \boldsymbol{M}_{\text{ps}}=\begin{bmatrix}0&0\\0&-M\omega^2\end{bmatrix},\quad \boldsymbol{K}_{\text{ps}}=\begin{bmatrix}0&0\\0&K_{\text{p}}\end{bmatrix},\quad C_{\text{ps}}=\begin{bmatrix}0&0\\0&-\mathrm{i}\omega\varepsilon_{\text{p}}\end{bmatrix}. \tag{28}$$

To proceed with the analysis, we have to evaluate the compliance matrix $\boldsymbol{\chi}_{\text{l-s}}^{-1}$, that is the coefficients J_{kj}. To this end it is convenient to introduce a new index of summation $l=m-n$ in Eq. (23) and rewrite it as

$$J_{kj}=\frac{1}{4\pi^2\tilde{\mu}}\int_{-\infty}^{\infty}\int_{-\infty}^{\infty}a_{kj}\frac{\sin k_1 b}{k_1 b}\frac{\sin k_2 a}{k_2 a}\sum_{l=-\infty}^{\infty}\exp(\mathrm{i}(k_1 d-q)l)\,\mathrm{d}k_1\,\mathrm{d}k_2. \tag{29}$$

Eq. (29) contains a double integration and an infinite summation. Accomplishing these operations numerically would be very laborious and inaccurate. Therefore, a preliminary analytical evaluation of this equation is necessary, which is shown in Appendix C and leads to the following expression

$$\begin{aligned}J_{jj}&=\frac{1}{4\pi\tilde{\mu}ab}\int_{-\infty}^{\infty}\frac{\sin k_2 a}{k_2}\left(a_{jj}(0,k_2,\omega)+2\sum_{m=1}^{\infty}\operatorname{res}\left\{\frac{a_{jj}(k_1,k_2,\omega)}{k_1}\right\}_{k_1=k_1^m}\right.\\&\quad\left.\times\left(\mathrm{e}^{\mathrm{i}k_1^m b}+\mathrm{i}\sin(k_1^m b)\frac{\cos q-\mathrm{e}^{\mathrm{i}k_1^m d}}{\cos(k_1^m d)-\cos q}\right)\right)\mathrm{d}k_2\\J_{13}&=\frac{\mathrm{i}}{2\pi\tilde{\mu}ab}\int_{-\infty}^{\infty}\frac{\sin k_2 a}{k_2}\sum_{m=1}^{\infty}\operatorname{res}\{a_{13}^0(k_1,k_2,\omega)\}_{k_1=k_1^m}\frac{\sin(k_1^m b)\sin q}{\cos(k_1^m d)-\cos q}\,\mathrm{d}k_2,\quad j=1,3.\end{aligned} \tag{30}$$

In order to analyze Eq. (30) numerically we should find the roots of equations $\cosh R_{\text{T}}H=0$ and $\Delta_0=0$ (see Eqs. (C.4)–(C.6)). The roots of the first equation ($\cosh R_{\text{T}}H=0$) can be easily found analytically to give:

$$k_1^m=\mathrm{i}\sqrt{\frac{\pi^2}{H^2}\left(m+\frac{1}{2}\right)^2+k_2^2-\frac{\omega^2}{\tilde{c}^2{}_{\text{T}}}}, \tag{31}$$

whereas the roots of the second equation ($\Delta_0=0$) can only be found numerically (using a program for finding complex roots of a transcendental equation). Having found all these roots, the residues in Eq. (30) can be calculated and summarized straightforwardly. Naturally, the summation should be carried out over a finite number of poles, which do not have very large imaginary and real parts (the contribution of the other terms into the sum is negligible). After the summation has been accomplished, only a well convergent integration over k_2 remains to be carried out to evaluate J_{kj}. This integration can be accomplished using a standard program for calculation of a single integral. Thus, we can consider J_{kj} as known complex functions of the angular frequency ω and the phase shift q.

Now that J_{kj} are known, Eq. (27) can be analyzed further. However, let us first study the equivalent dynamic $\boldsymbol{\chi}_{\text{l-s}}$. This study will be limited by considering the vertical component of the stiffness, which is most influential for the vertical dynamics of the railway track. To find an expression for this component, the stiffness of the longitudinal contact between the layer and sleepers should be disregarded. In this case, the

matrix Eq. (27) can be reduced to the following algebraic equation that describes the vertical vibrations of the sleepers:

$$C(\chi_{\mathrm{l-s}}^{\mathrm{vert}} - M\omega^2 + K_{\mathrm{p}} - \mathrm{i}\omega\varepsilon_{\mathrm{p}}) = C_0(K_{\mathrm{p}} - \mathrm{i}\omega\varepsilon_{\mathrm{p}}) \tag{32}$$

with

$$\chi_{\mathrm{l-s}}^{\mathrm{vert}} = -1/J_{33}. \tag{33}$$

It is easy to see that Eq. (32) describes the vertical motion of a sleeper in the frequency domain as shown in Fig. 3 (the sleeper is presented by a black rectangle).

The stiffness $\chi_{\mathrm{l-s}}^{\mathrm{vert}}$ in Eqs. (32) and (33) and in Fig. 3 is, obviously, the vertical equivalent stiffness of the layer at the contact points with the sleepers. It is important to underline that this stiffness does not depend on the number n of the sleeper, i.e. the layer under each sleeper can be replaced by a *set of identical springs* with complex stiffness $\chi_{\mathrm{l-s}}^{\mathrm{vert}}$.

As follows from Eqs. (33) and (30), the equivalent vertical stiffness $\chi_{\mathrm{l-s}}^{\mathrm{vert}}$ is given as

$$\chi_{\mathrm{l-s}}^{\mathrm{vert}} = -\left(\frac{1}{4\pi\tilde{\mu}ab} \int_{-\infty}^{\infty} \frac{\sin k_2 a}{k_2} \left(a_{33}(0,k_2,\omega) + 2\sum_{m=1}^{\infty} \mathrm{res}\left\{ \frac{a_{33}(k_1,k_2,\omega)}{k_1} \right\}_{k_1=k_1^m} \right.\right.$$
$$\left.\left. \times \left(\mathrm{e}^{\mathrm{i}k_1^m b} + \mathrm{i}\sin(k_1^m b) \frac{\cos q - \mathrm{e}^{\mathrm{i}k_1^m d}}{\cos(k_1^m d) - \cos q} \right) \right) \mathrm{d}k_2 \right)^{-1} \tag{34}$$

and, therefore, is a complex-valued function of frequency ω and the phase shift q between vibrations of neighboring supports.

The result of numerical evaluation of Eq. (34) is presented in Fig. 4. The equivalent stiffness is shown in this figure as a function of frequency ω for the fixed value of the phase shift $q = \omega d/V$ equal to 0.5. The solid and the dashed lines in Fig. 4 correspond to the real and imaginary parts of $\chi_{\mathrm{l-s}}^{\mathrm{vert}}$, respectively.

The calculations were carried out using the following parameters

for the layer

$$\mu = 2.6 \times 10^7\ \mathrm{N/m^2}, \quad \rho = 1960\ \mathrm{kg/m^3}, \quad \nu = 0.3, \quad \mu^* = 2.6 \times 10^4\ \mathrm{N\,s/m^2}, \quad H = 5\ \mathrm{m}, \tag{35}$$

for the sleepers (*geometrical parameters only*)

$$2a = 2.7\ \mathrm{m}, \quad d = 0.6\ \mathrm{m}, \quad 2b = 0.27\ \mathrm{m}. \tag{36}$$

Parameters of the layer given by Eq. (35) are almost identical to those used by Metrikine et al. (2001). These parameters describe a realistic, quite stiff ground with the Rayleigh wave speed of $c_{\mathrm{R}} = 384$ km/h, shear wave speed of $c_{\mathrm{T}} = 414$ km/h, and dilatational wave speed of $c_{\mathrm{L}} = 775$ km/h. The geometric parameters of the sleepers are common for Western European railways.

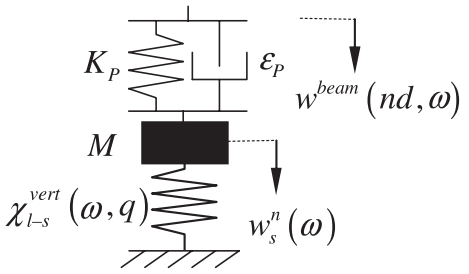

Fig. 3. Equivalent model for vertical motion of a sleeper (frequency domain).

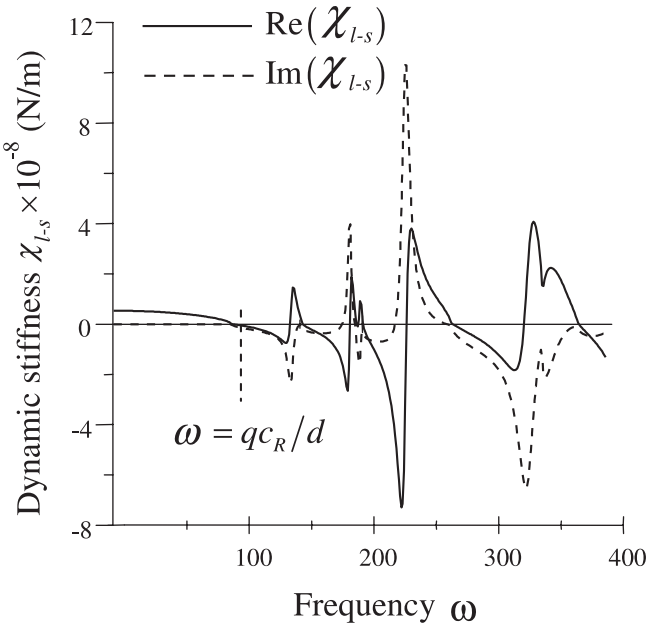

Fig. 4. Equivalent stiffness of the layer versus angular frequency for $q = \omega d/V = 0.5$.

Fig. 4 shows that the equivalent stiffness is a complicated function of frequency. For frequencies smaller than $\omega = qc_R/d$, the real part of the equivalent stiffness is positive and the imaginary part, although not zero, is very small. This implies that at this frequency band, for a fixed q, vibrations of the supports generate no waves in the layer. For frequencies close to $\omega = qc_R/d$ the equivalent stiffness becomes very small. This happens because of the Rayleigh waves, which are generated so that they arrive to every sleeper in phase (resonance), providing a large displacement of the layer under the sleepers (see Metrikine and Popp, 1999). Fig. 4 shows also that the equivalent stiffness can be quite large at some frequencies. This effect can be considered as "anti-resonance", which occurs if waves, as well as exponentially decaying displacement fields, generated by the sleepers, are almost in anti-phase under any support, resulting in small displacements of the layer under the sleepers. The frequencies that correspond to these large values of χ_{l-s}^{vert} cannot be found analytically since all three waves in the layer as well as the decaying displacement fields take part in the phenomenon of anti-resonance.

The most important conclusion to be drawn from analysis of the equivalent stiffness is that χ_{l-s}^{vert} can be very small at some frequencies, which are determined by the equation $\omega = qc_R/d$. Because of this, a uniform motion of a constant load with a velocity that is equal to the Rayleigh wave speed can cause resonance in the structure. Indeed, the phase shift between vibrations of the neighboring sleepers $q(\omega)$ in the case of a constant load is given by expression (24). Correspondingly, the condition for the equivalent stiffness to be small takes the form

$$\frac{\omega d}{c_R} = \frac{\omega d}{V}. \tag{37}$$

Thus, if the load velocity becomes equal to the Rayleigh wave speed, that is $V = c_R$, the layer reaction becomes very small at all frequencies. As a result, vibrations of the beam that are generated by such load should have large amplitude. Thus, the Rayleigh wave velocity is critical for the model at hand.

Maximums of the equivalent stiffness should not be forgotten as well. They also distinguish clearly the equivalent stiffness $\chi_{\mathrm{l-s}}^{\mathrm{vert}}$ from a constant stiffness, which is frequently used in literature to replace the ground reaction.

3.2. Steady-state response of the beam

In this section, the steady-state response of the rail (beam) is found and studied. This response is governed by Eqs. (14), (21) and (22), which form the following system of equations

$$\begin{aligned} &E_{\mathrm{beam}} I \partial_{xxxx} w_{\omega}^{\mathrm{beam}}(x,\omega) - \rho_{\mathrm{beam}} S \omega^2 w_{\omega}^{\mathrm{beam}}(x,\omega) \\ &\quad = -\frac{2\pi P}{V} \mathrm{e}^{\mathrm{i}x(\omega/V)} \left(1 + \mathrm{e}^{\mathrm{i}d_1(\omega/V)} + \mathrm{e}^{\mathrm{i}(d_1+d_2)(\omega/V)} + \mathrm{e}^{\mathrm{i}(2d_1+d_2)(\omega/V)}\right) \\ &\qquad + \sum_{n=-\infty}^{\infty} [(K_{\mathrm{p}} - \mathrm{i}\omega\varepsilon_{\mathrm{p}})(w(nd,0,0,\omega) - w^{\mathrm{beam}}(nd,\omega))]\delta(x-nd), \end{aligned} \tag{38}$$

$$\begin{aligned} &w_{\omega}^{\mathrm{beam}}(nd,\omega) = C_0(\omega)\exp(\mathrm{i}\omega nd/V), \\ &w_{\omega}(nd,0,0,\omega) = C(\omega)\exp(\mathrm{i}\omega nd/V), \\ &u_{\omega}(nd,0,0,\omega) = A(\omega)\exp(\mathrm{i}\omega nd/V), \end{aligned} \tag{39}$$

$$\begin{aligned} &A(\omega) = KJ_{11}A(\omega) + J_{13}(C_0(\omega)(K_{\mathrm{p}} - \mathrm{i}\omega\varepsilon_{\mathrm{p}}) + (-M\omega^2 + K_{\mathrm{p}} - \mathrm{i}\omega\varepsilon_{\mathrm{p}})C(\omega)), \\ &C(\omega) = KJ_{31}A(\omega) + J_{33}(C_0(\omega)(K_{\mathrm{p}} - \mathrm{i}\omega\varepsilon_{\mathrm{p}}) + (-M\omega^2 + K_{\mathrm{p}} - \mathrm{i}\omega\varepsilon_{\mathrm{p}})C(\omega)). \end{aligned} \tag{40}$$

This system can be simplified by eliminating $A(\omega)$ from Eq. (40) and substituting $w_{\omega}(nd,0,0,\omega)$ and $w_{\omega}^{\mathrm{beam}}(nd,\omega)$ into Eq. (38). This yields

$$\begin{aligned} &E_{\mathrm{beam}} I \partial_{xxxx} w_{\omega}^{\mathrm{beam}}(x,\omega) - \rho_{\mathrm{beam}} S \omega^2 w_{\omega}^{\mathrm{beam}}(x,\omega) \\ &\quad = -\frac{2\pi P}{V} \mathrm{e}^{\mathrm{i}x(\omega/V)} \left(1 + \mathrm{e}^{\mathrm{i}d_1(\omega/V)} + \mathrm{e}^{\mathrm{i}(d_1+d_2)(\omega/V)} + \mathrm{e}^{\mathrm{i}(2d_1+d_2)(\omega/V)}\right) \\ &\qquad - C_0(\omega)(K_{\mathrm{p}} - \mathrm{i}\omega\varepsilon_{\mathrm{p}})B_0(\omega) \sum_{n=-\infty}^{\infty} \exp(\mathrm{i}\omega nd/V)\delta(x-nd), \\ &w_{\omega}^{\mathrm{beam}}(nd,\omega) = C_0(\omega)\exp(\mathrm{i}\omega nd/V), \end{aligned} \tag{41}$$

where

$$B_0 = -M\omega^2 - 1/J_{33} + K_{\mathrm{p}} - \mathrm{i}\omega\varepsilon_{\mathrm{p}} + \frac{KJ_{13}J_{31}}{J_{33}(J_{33}(1-KJ_{11}) + KJ_{13}J_{31})}. \tag{42}$$

For the analysis to follow, it is convenient to rewrite Eq. (41) making no use of the Dirac delta-function. This can be accomplished employing the relationship between the classical and generalized derivatives (Vladimirov, 1979) to give

$$E_{\mathrm{beam}} I \frac{\partial^4}{\partial x^4} w_{\omega}^{\mathrm{beam}}(x,\omega) - \rho_{\mathrm{beam}} S \omega^2 w_{\omega}^{\mathrm{beam}}(x,\omega) = -\frac{2\pi P}{V} \mathrm{e}^{\mathrm{i}x(\omega/V)} \left(1 + \mathrm{e}^{\mathrm{i}d_1(\omega/V)} + \mathrm{e}^{\mathrm{i}(d_1+d_2)(\omega/V)} + \mathrm{e}^{\mathrm{i}(2d_1+d_2)(\omega/V)}\right), \tag{43}$$

$$\begin{aligned} &[w_{\omega}^{\mathrm{beam}}]_{x=nd} = [\partial_x w_{\omega}^{\mathrm{beam}}]_{x=nd} = [\partial_{xx} w_{\omega}^{\mathrm{beam}}]_{x=nd} = 0, \\ &E_{\mathrm{beam}} I [\partial_{xxx} w_{\omega}^{\mathrm{beam}}]_{x=nd} = -C_0(\omega)B_0(\omega)\exp(\mathrm{i}\omega nd/V), \end{aligned} \tag{44}$$

$$w_{\omega}^{\text{beam}}(nd,\omega) = C_0(\omega)\exp(\mathrm{i}\omega nd/V), \tag{45}$$

where the square brackets denote the following difference: $[f(x)]_{x=a} = f(x=a+0) - f(x=a-0)$. Eq. (43) describes the vertical motion of the beam under the moving loads in all points everywhere but not at the supported points. At these points, the boundary conditions given by Eqs. (44) and (45) are to be employed.

To find the steady-state solution to the system of Eqs. (43)–(45) we employ a method, which is based on the fact that the beam displacement in the frequency domain satisfies the following condition (in application to 1D structures this method was used, for example, by Vesnitskii and Metrikine, 1996; Belotserkovskiy, 1996):

$$w_{\omega}^{\text{beam}}(x+d,\omega) = w_{\omega}^{\text{beam}}(x,\omega)\exp\left(\mathrm{i}d\frac{\omega}{V}\right). \tag{46}$$

This condition can be validated by direct substitution into Eqs. (43)–(45).

Condition (46) is commonly referred to as the *periodicity condition*. It gives a relationship between the beam displacements at the points that are separated by the span distance d. Physically, this condition implies that in the steady-state regime the beam displacement is repeated in time with the period $T = d/V$ but with translation in space equal to d.

The periodicity condition (46) allows to obtain the solution to the problem (43)–(45) by performing the following three steps.

1. The general solution to Eq. (43) is to be written in the interval $x \in [0,d]$. This solution contains four unknown constants C_i, $i = 1,\ldots,4$.
2. Using the periodicity condition, the solution in the interval $x \in [d,2d]$ can be obtained from that in the interval $x \in [0,d]$ by multiplying the latter by $\exp(\mathrm{i}d\omega/V)$. Obviously, the result of this multiplication contains the same four constants C_i, $i = 1,\ldots,4$.
3. Four unknown constants C_i, $i = 1,\ldots,4$ and one extra constant that is related to the Fourier-displacement of the sleeper number $n = 1$ are to be found by employing five boundary conditions at the point $x = d$ given by Eqs. (44) and (45).

Let us accomplish this way of solution. The general solution to Eq. (43) in the interval $x \in [0,d]$ can be written as

$$w_{\omega}^{\text{beam}}(x,\omega) = C_1\exp(\alpha x) + C_2\exp(-\alpha x) + C_3\exp(\mathrm{i}\alpha x) + C_4\exp(-\mathrm{i}\alpha x) - F_0\exp\left(\mathrm{i}x\frac{\omega}{V}\right), \tag{47}$$

with

$$\alpha = (\rho_{\text{beam}}/E_{\text{beam}}I)^{1/4}, \quad F_0 = \frac{2\pi PV^3}{E_{\text{beam}}I\omega^4 - \rho\omega^2}\left(1 + \mathrm{e}^{\mathrm{i}d_1\frac{\omega}{V}} + \mathrm{e}^{\mathrm{i}(d_1+d_2)(\omega/V)} + \mathrm{e}^{\mathrm{i}(2d_1+d_2)(\omega/V)}\right), \tag{48}$$

and $C_j (j = 1,\ldots,4)$ unknown constants.

In accordance with the periodicity condition (46), the general solution to Eq. (43) in the interval $x \in [d,2d]$ can be expressed as

$$\begin{aligned} w_{\omega}^{\text{beam}}(x,\omega) = \exp\left(\mathrm{i}d\frac{\omega}{V}\right)\{&C_1\exp(\alpha(x-d)) + C_2\exp(-\alpha(x-d)) + C_3\exp(\mathrm{i}\alpha(x-d)) \\ &+ C_4\exp(-\mathrm{i}\alpha(x-d))\} - F_0\exp\left(\mathrm{i}x\frac{\omega}{V}\right). \end{aligned} \tag{49}$$

Substitution of Eqs. (47) and (49) into the boundary conditions (44) and (45) gives a system of five algebraic equations, which is presented in Appendix D together with its analytical solution (Eqs. (D.1) and (D.2), respectively).

Thus, the steady-state displacement of the beam is found in the frequency domain. In the interval $x \in [0, d]$ this displacement is determined by Eqs. (47) and (D.2). For other values of the co-ordinate x, the periodicity condition (46) is to be applied.

The beam displacement in the time domain can be found numerically applying the inverse Fourier transform to Eq. (47). In the interval $x \in [0, d]$ this yields

$$w^{\text{beam}}(x,t) = \frac{1}{2\pi}\int_{-\infty}^{\infty}\left(C_1 e^{\alpha x} + C_2 e^{-\alpha x} + C_3 e^{i\alpha x} + C_4 e^{-i\alpha x} - F_0 e^{ix(\omega/V)}\right)e^{-i\omega t}\,d\omega. \tag{50}$$

The further analysis will be carried out in the following way. First, the beam response will be studied to a single load that is located at the point $x = Vt$ (the other loads will be disregarded). Under this single load, (a) the beam displacement at the loading point will be studied as a function of the load velocity; (b) the effect of the damping in the layer and supports (pads) on the displacement of the beam at this point will be investigated. To study importance of modeling the sleepers as *discretely* positioned supports, this displacement will be compared to that of a corresponding homogenized model. Second, the beam profiles corresponding to a single load, two loads (bogie) and four loads (wagon) will be elaborated.

The beam deflection is calculated using parameters of the structure given by Eqs. (35) and (36). Additionally, the following parameters for the beam, load and pads are employed (these parameters correspond to UIC60 rail and a train's wheel loading)

$$\begin{aligned} &E_{\text{beam}}I = 6.11\times 10^6\ \text{N m}^2, \quad \rho_{\text{beam}}S = 60.34\ \text{kg/m}, \quad P = 100\ \text{kN},\\ &M = 250\ \text{kg}, \quad K_{\text{p}} = 10^8\ \text{N/m}, \quad \varepsilon_{\text{p}} = 10^5\ \text{N s/m}. \end{aligned} \tag{51}$$

For comparison, the beam deflection is calculated on the basis of a correspondent homogenized model, in which (a) the sleepers and the pads are considered as being uniformly distributed along the beam; (b) the contact between the sleepers and the surface of the layer is considered to take place everywhere within the area $|y| < a$. The homogenized model is very similar to that considered by Sheng et al. (1999). To have an exact correspondence between the original and homogenized models, parameters of the latter should be taken as

$$M^{\text{hom}} = \frac{M}{d}, \quad K_{\text{P}}^{\text{hom}} = \frac{K_{\text{P}}}{d}, \quad \varepsilon_{\text{P}}^{\text{hom}} = \frac{\varepsilon_{\text{P}}}{d}. \tag{52}$$

Fig. 5 presents the beam displacement at the loading point as a function of the load velocity for two values of the material damping in the layer. The solid line corresponds to the periodically inhomogeneous model, whereas the dashed line is related to the homogenized one. For the inhomogeneous model, the displacement is calculated at the time moment when the load passes the sleeper $n = 0$ ($x_{\text{load}} = 0$). [1]

Fig. 5 shows that the velocity dependence of the beam deflection is almost the same for both models. Slight difference takes place at small velocities and in the vicinity of the critical velocity ($V = 390$ km/h). The latter is larger than the Rayleigh wave velocity and smaller than the shear wave velocity ($c_{\text{R}} = 384$ km/h, $c_{\text{T}} = 414$ km/h).

Fig. 6 shows the effect of the damping in the pads on the beam displacement at the loading point, which is perceptible as follows from the figure. The larger the damping the smaller the beam deflection. It should be mentioned, however, that the smaller the material damping in the layer the less sensitive the beam response to the damping in the pads.

The characteristic beam profiles are presented in Fig. 7 under the single load, two loads (bogie) and four loads (wagon), respectively. The profiles are plotted for three values of the load velocity: 250 km/h ($V < c_{\text{R}}$), 400 km/h ($c_{\text{T}} < V < c_{\text{L}}$) and 500 km /h ($c_{\text{T}} < V < c_{\text{L}}$). These velocities are chosen to represent

[1] Calculations show that the beam deflection at the loading point depends only slightly on the load position.

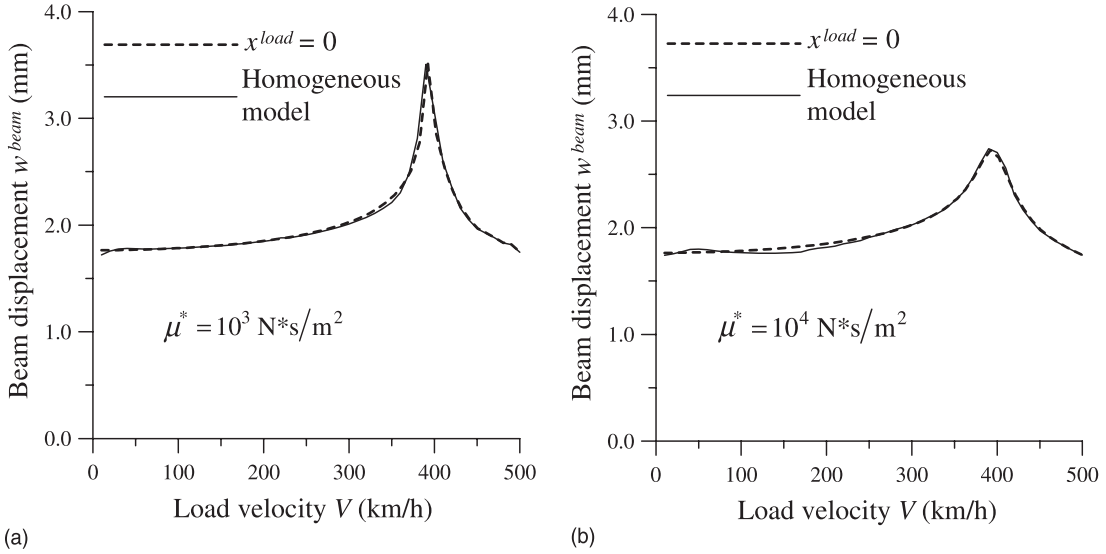

Fig. 5. Displacement of the beam at the loading point versus load velocity. Effect of material damping.

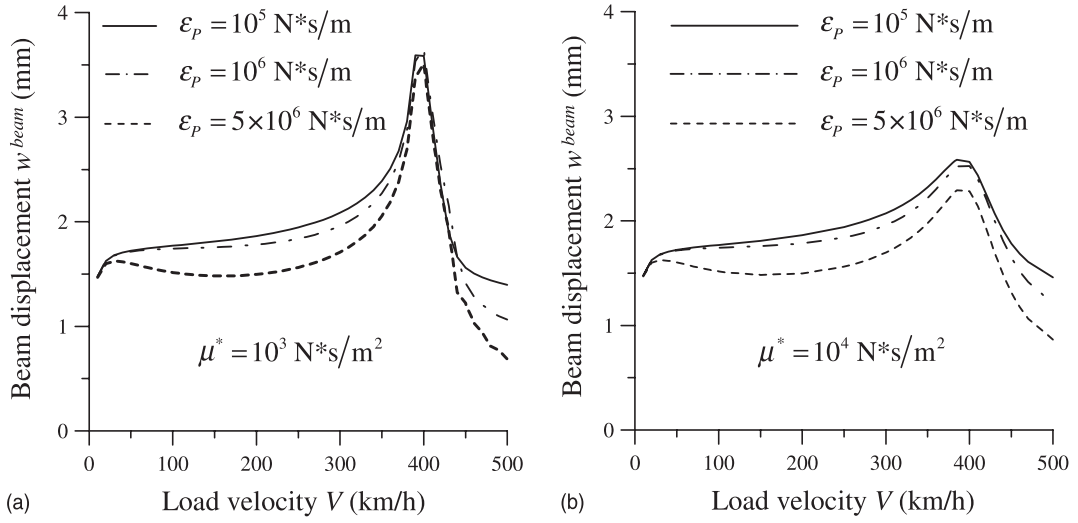

Fig. 6. Displacement of the beam at the loading point versus load velocity. Combined effect of material damping and viscosity of the pads.

three regimes of motion. The velocity of 250 km/h corresponds to the sub-critical regime and is a characteristic velocity of contemporary Western-European high-speed trains. The velocity 400 km/h is representative for the near-critical response of the beam. As for the last velocity, 500 km/h, this is about the record for modern trains.

The displacements are calculated at the time moment when the front load ($x = Vt$) is at the point $x = 0$, i.e. exactly above the sleeper $n = 0$. For the distances between the loads, the dimensions of German ICE are adopted:

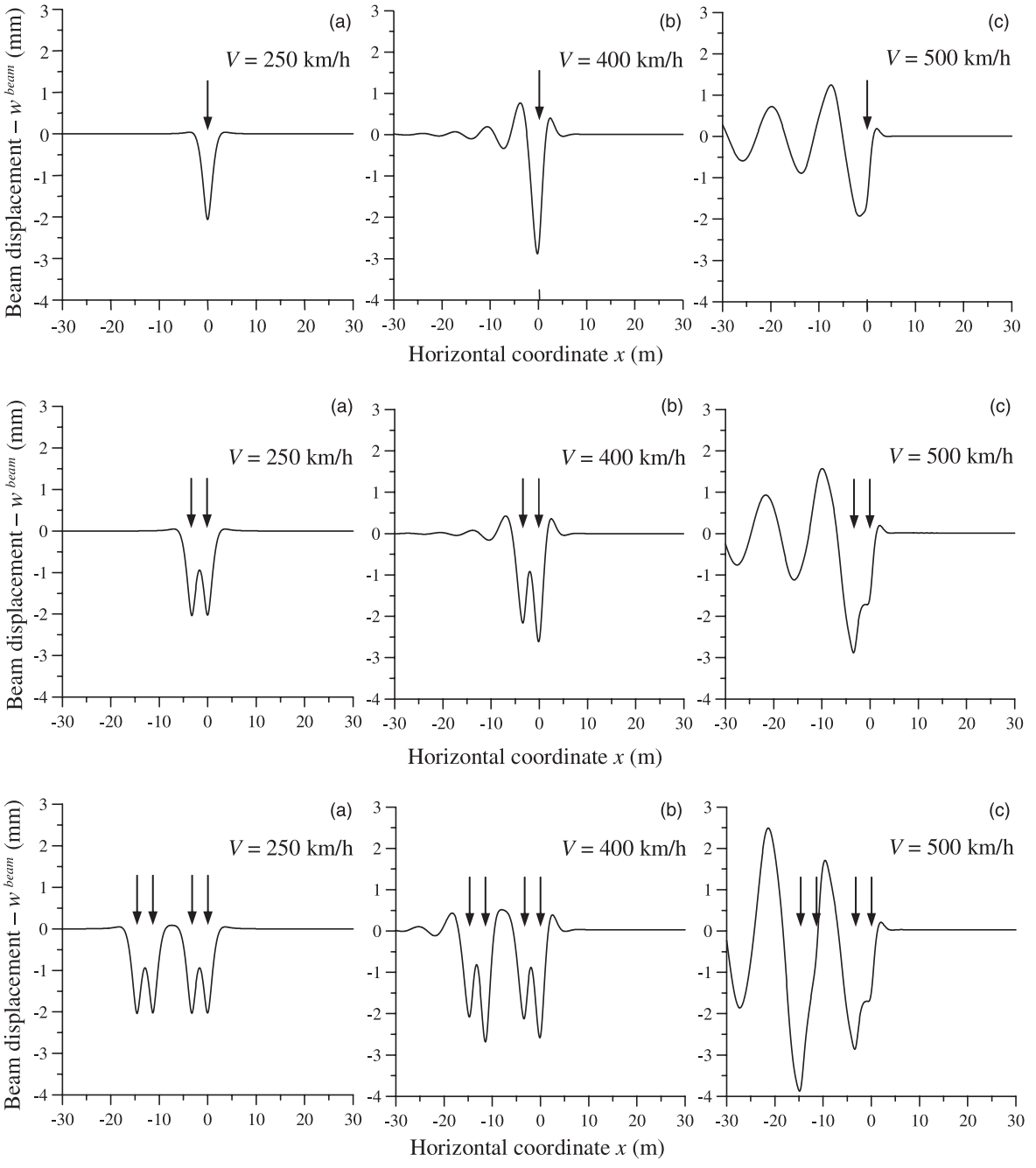

Fig. 7. Beam patterns.

$$d_1 = 3 \text{ m}, \quad d_2 = 8.46 \text{ m}. \tag{53}$$

Here d_1 is the bogie wheelbase, d_2 is the distance between two car bogies (see Fig. 2).

Fig. 7(a) show that in the sub-critical motion the loads generate no waves in the system. The response is almost symmetric with respect to the loads. A small asymmetry is introduced by the damping in the pads and the layer.

In the supercritical motion, the loads excite waves in the beam. The length of these waves can be in the order of the bogie wheelbase d_1 and the car distance d_2. Interfering between each other, these waves can result either in decrease or increase of the maximum displacement of the beam as compared to the case of a single load.

Let is note that the beam profiles are not stationary in the reference system that moves with the load. They constantly change in time since the structure is inhomogeneous. However, thanks to periodic character of inhomogeneity and uniformity of motion of the load, the profiles repeat themselves in time with the period $T = d/V$.

4. Elastic drag experienced by a train due to excitation of ground vibrations

In this section, we investigate a so-called "elastic drag" experienced by a train. This drag was introduced by Metrikine et al. (2001) as a measure for energy loss that the train experiences due to excitation of waves in the track and surrounding soil. First, we will analyze the elastic drag for a single load. Then, the influence of the bogie wheelbase on the drag will be studied considering two loads. Finally, the elastic drag experienced by a high-speed train (French TGV) will be calculated and compared to the drag, which is predicted by corresponding homogenized model.

According to Metrikine et al. (2001), in the case of a constant loading the elastic drag can be calculated as a ratio between the power input Q (energy per unit time that is transmitted into elastic system by the moving load) and the load velocity V. For the case of a single load (wheel) the power input is given as

$$D_{\mathrm{e}}^{\mathrm{wheel}} = \frac{Q}{V} = \frac{P}{V}\left.\frac{\partial w^{\mathrm{beam}}}{\partial t}\right|_{x=Vt}. \tag{54}$$

Results of numerical evaluation of Eq. (54) are presented in Fig. 8 that shows the dependence of the elastic drag $D_{\mathrm{e}}^{\mathrm{wheel}}$ on the load velocity V at the moment $t = 0$, when the load passes the sleeper $n = 0$. The figure presents three curves that are plotted for three values of the material damping μ^*. The other parameters are given by Eqs. (35), (36) and (51).

Fig. 8 shows that the elastic drag grows rapidly as the load velocity approaches the critical one. This result is in perfect correspondence with that obtained by Metrikine et al. (2001) on the basis of a homogeneous model. The specific feature of the drag in the periodically inhomogeneous model is that the drag is a periodic, with the period $T = d/V$, function of time (not a constant as for homogeneous models). Therefore, to obtain a physically relevant value, the drag should be averaged with respect to the sleeper period using the following expression

$$\overline{D}_{\mathrm{e}}^{\mathrm{wheel}} = \frac{P}{Vd}\int_0^d \left.\frac{\partial w^{\mathrm{beam}}}{\partial t}\right|_{t=x/V} \mathrm{d}x. \tag{55}$$

For a single load, however, $D_{\mathrm{e}}^{\mathrm{wheel}}$ and $\overline{D}_{\mathrm{e}}^{\mathrm{wheel}}$ appear to be almost the same. Therefore, Fig. 8 is representative for $\overline{D}_{\mathrm{e}}^{\mathrm{wheel}}$ as well.

Consider now the elastic drag experienced by two loads moving at a fixed distance d_1 from each other (bogie). This drag is given as

$$D_{\mathrm{e}}^{\mathrm{bogie}} = \frac{P}{V}\left(\left.\frac{\partial w^{\mathrm{beam}}}{\partial t}\right|_{x=Vt} + \left.\frac{\partial w^{\mathrm{beam}}}{\partial t}\right|_{x=Vt-d_1}\right). \tag{56}$$

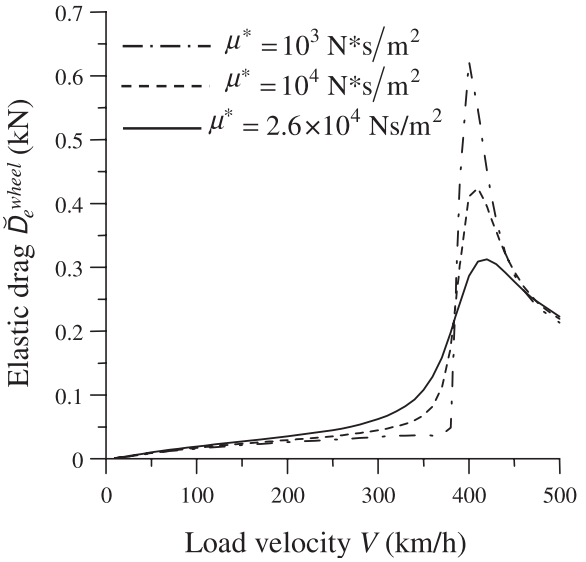

Fig. 8. Elastic drag for a single load versus load velocity.

To study the effect of the bogie wheelbase d_1, D_e^{bogie} is plotted in Fig. 9 as a function of d_1 for two velocities of the loads. Fig. 9(a) presents the drag at the time moment $t = 0$, whereas Fig. 9(b) shows the drag at $t = d/2V$. Fig. 9 demonstrates the following:

(1) Elastic drag in the sub-critical case (250 km/h) is less than that in the supercritical one (400 km/h).
(2) Dependence of the elastic drag on the wheelbase has a minimum located approximately at $d = 2$ m.

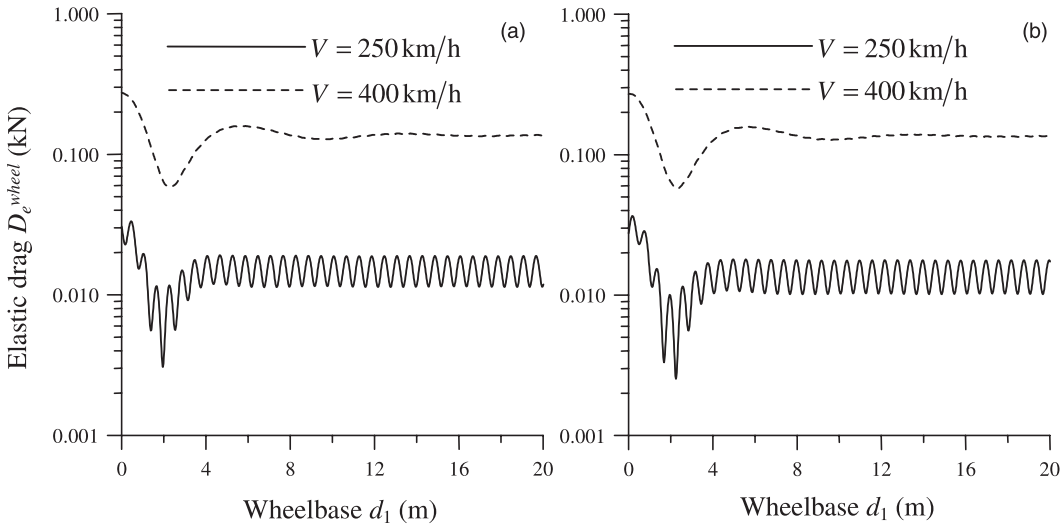

Fig. 9. Elastic drag for a car's bogie versus wheelbase; (a) $x = 0$; (b) $x = d/2$.

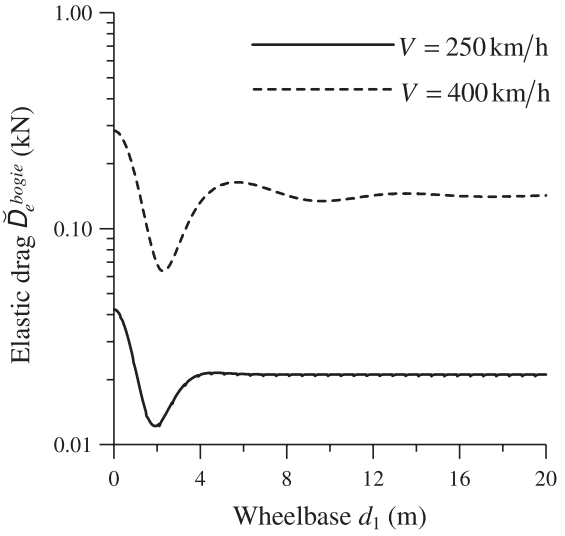

Fig. 10. Elastic drag averaged over the sleeper distance versus wheelbase.

(3) Elastic drag experienced by a bogie depends upon the wheelbase and is quite sensitive to variation of this distance, especially in the sub-critical motion. This is a consequence of the periodicity of the structure.
(4) Elastic drag depends on the time moment, at which it is calculated.

Let us study the average value of the drag experienced by two loads, which is given by the following expression and shown in Fig. 10

$$\overline{D}_{\mathrm{e}}^{\mathrm{bogie}} = -\frac{P}{Vd}\int_0^d \left(\left.\frac{\partial w^{\mathrm{beam}}}{\partial t}\right|_{x=Vt} + \left.\frac{\partial w^{\mathrm{beam}}}{\partial t}\right|_{x=Vt-d_1} \right) \mathrm{d}x. \tag{57}$$

This figure shows that the averaging removes the oscillatory dependence of the drag on the wheelbase d_1. Additionally, as the distance d_1 exceeds 10 m, the drag becomes almost independent of this distance. This implies that the drag experienced by two bogies of one wagon can be found by simple doubling of the drag experienced by one bogie.

Consider the drag experienced by a high-speed train taking as an example a TGV, which consists of two power cars and eight passenger cars. The weight of the power car is 80,000 kg, the weight of the passenger car is 40,000 kg. Thus, each wheelset of the power cars corresponds to the loading of 200,000 N whereas each wheelset of a passenger car gives 100,000 N of constant loading. Geometric parameters of the TGV are

$$d_1 = 3 \text{ m}, \quad d_2 = 11 \text{ m}, \quad d_3 = 3.27 \text{ m}, \tag{58}$$

where d_1 is the bogie wheelbase, d_2 is the distance between the last wheelset of the first bogie and the first wheelset of the second bogie, and d_3 is the distance between the last wheelset of the first wagon and the first wheelset of the second wagon (see Fig. 2).

In the paper of Metrikine et al. (2001) it was concluded that the elastic drag is small with respect to the aerodynamic drag. This conclusion, however, was drawn considering the contact force between the wheels of the train and the rails as given by the dead weight of the train alone. No dependence of the contact force on the velocity of the train was accounted for. In reality, the contact force depends on the aerodynamic resistance to the train motion. Thanks to the special design of high-speed trains, this resistance presses the

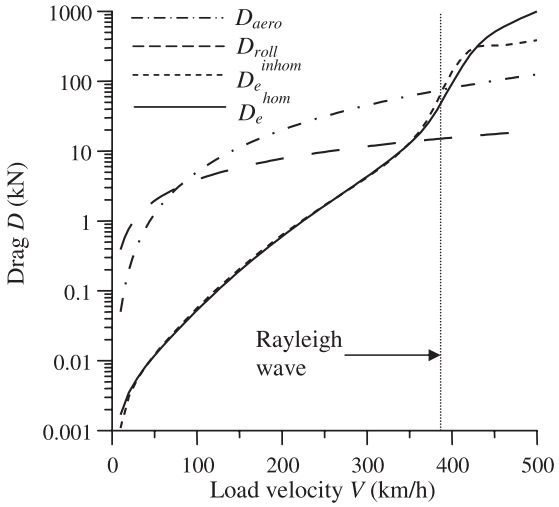

Fig. 11. Elastic drag for inhomogeneous model (D_e^{inhom}), elastic drag for homogenised model (D_e^{hom}), rolling drag (D_{roll}), and aerodynamic drag (D_{aero}) versus load velocity.

train, especially the first wagon (locomotive) against the rails. We are not aware of any measurements of the aerodynamically induced contact pressure. Therefore, we model it in a rough way, by replacing the weight of the locomotive P by $P(1+\gamma V^2)$, where γ is a coefficient, which reflects the fact that the aerodynamic drag (which is normally assumed as being proportional to V^2) influences the contact force between the train wheels and the rails. This coefficient depends on the shape of a high-speed train and the surface of the train as any drag coefficient associated with a flow around a body.

To show possible effect of the aerodynamically induced contact force on the elastic drag, we calculated the latter assuming that $\gamma = 0.001\ s^2/m^2$. Considering only the wheels of the power car being subjected to the effect of the aerodynamic pressure, and employing parameters given by Eqs. (35), (36), (51) and (58), the elastic drag was calculated for the TGV. The result is shown in Fig. 11 in the form of dependence of the drag on the train velocity.

To compare the periodically inhomogeneous model to the correspondent homogenized model, the velocity dependence of the elastic drag for the latter is also shown in Fig. 11. The aerodynamic drag and the rolling drag are plotted in accordance with the results of paper (Hopkins et al., 1999).

Comparing the inhomogeneous and homogenized models, one can conclude that the difference between them becomes apparent in the supercritical regime only, in which the elastic drag for the homogenized model is larger.

The most important result that is demonstrated by Fig. 11 is that as soon as the train velocity approaches the Rayleigh wave speed, the elastic drag becomes comparable with the aerodynamic drag and then exceeds it. Thus, in the opinion of the authors, one of the design criteria for high-speed trains should be the energy consumption calculated on the basis of the aerodynamic, rolling and elastic drag. The latter should be included necessarily, being a possible cause of perceptible energy loss.

5. Discussion and conclusions

In this paper, the dynamic response of a railway track to a moving train has been studied employing a three-dimensional model for the track. The model has been composed of two beams on periodically

positioned supports and a visco-elastic layer. Every support has been assumed to contact the layer over a rectangular area, within which the surface tractions have been uniformly distributed. The train loading has been accounted for with the help of a set of vertical point loads applied to the beams. Both the magnitude and translational (along the beams) velocity of these loads has been chosen as constant.

The aim of the paper has been to present a method of quasi-analytical analysis of dynamic response of the track and to consider a number of issues associated with the dynamic behavior of the track, which have not received enough attention in the past. These issues are: (a) the effect of periodic inhomogeneity of the track (introduced by sleepers) on its dynamic response; (b) the relevance of "elastic drag", which the train experiences because of excitation of the track and ground vibrations. To enable consideration of the first issue, a homogenized model has been employed for comparison, the homogenization applied to the sleepers making them uniformly and continuously distributed along the track.

It has been shown that the homogenized model predicts almost the same response as the original inhomogeneous model. Both models predict a critical velocity of the train, which, for the chosen model of the ground, is larger than the Rayleigh wave velocity and smaller than the shear wave velocity. The material damping in the layer and viscosity in the pads (elements that are positioned between the rails and sleepers), which effect the track response significantly, have shown to influence both models equivalently.

The elastic drag for a TGV has been calculated and compared to the aerodynamic and rolling drag. It has been shown that at high velocities of the train (close to the Rayleigh wave speed) the elastic drag is comparable to or larger than the aerodynamic drag. Thus, the elastic drag can be a cause of considerable energy consumption.

Let us discuss the results obtained in this paper. To our knowledge, this paper is the first attempt to show that the periodically inhomogeneous, three-dimensional model for a railway track predicts almost the same dynamic response of the rails as a corresponding homogenized model. This result can be quite valuable for railway engineers, since the homogenized model needs much less calculation time than the inhomogeneous one. We ought to note, however, that validity of the homogenized model has been proven in this paper for the loads of constant magnitude only. Therefore, the homogenized model might fail if a varying in time load or a system with internal degrees of freedom would be employed to model the train.

The elastic drag that has been calculated in this paper might become an important issue in the years to come, since it is concerned with energy consumption, which is a key issue nowadays. We do not possess enough date to prove that the elastic drag is indeed as relevant as the aerodynamic drag. However, a rough estimation of the elastic drag, which has been presented in this paper, indicates importance of a further investigation of this drag. Assuming that the elastic drag can be indeed as high as predicted in this paper, we should think of measures to reduce it. A few ways to accomplish this are discussed below.

The most decisive way to decrease the elastic drag and to avoid the dynamic amplification in general is to increase the critical velocity along the railway track. This can be achieved by (a) embedding the track in a concrete slab (so-called slab track); (b) building the track on piles thereby uncoupling vibrations of the track from those of the ground.

A less decisive but easy way to reduce the elastic drag is a redistribution of the train weight. Indeed, the elastic drag is proportional to the train's weight squared. This implies that contribution of heavy wagons is considerably larger than that of more lightweight wagons. Thus, uniform distribution of the weight over the train length can reduce the elastic drag significantly. Note that although because of other reasons, the last generation of German ICE has engines mounted to every wagon, not only to the locomotive(s).

One more option to reduce the elastic drag lays in its dependence on the wheelbase of the train bogie. Varying this wheelbase within reasonable limits, the drag can be reduced by factor two.

Finalizing the paper, it should be noted once again that the mathematical formulation of the problem that has been used in this paper is approximate because of the assumption of uniform distribution of stresses beneath the sleepers. The only way to validate this assumption is to compare results obtained in this paper to those of a direct numerical simulation of a corresponding mixed contact problem. We are going to carry out this comparison in the nearest future.

Acknowledgements

This work was partly financed by the Russian Foundation for Basic Research, grants 03–01–00644 and 03–01–06184. This support is highly appreciated.

Appendix A

The expressions for the displacement vector $\boldsymbol{u}$ and stresses σ_{zz}, τ_{zx}, τ_{zy} in terms of the potentials φ and $\boldsymbol{\psi}$ read (see Achenbach, 1973)

$$u = \frac{\partial\varphi}{\partial x} + \frac{\partial\psi_z}{\partial y} - \frac{\partial\psi_y}{\partial z}, \quad v = \frac{\partial\varphi}{\partial y} - \frac{\partial\psi_z}{\partial x} + \frac{\partial\psi_x}{\partial z}, \quad w = \frac{\partial\varphi}{\partial z} + \frac{\partial\psi_y}{\partial x} - \frac{\partial\psi_x}{\partial y}, \tag{A.1}$$

$$\sigma_{zz} = \hat{\lambda}\nabla^2\varphi + 2\hat{\mu}\left(\frac{\partial^2\varphi}{\partial z^2} + \frac{\partial}{\partial z}\left(\frac{\partial\psi_y}{\partial x} - \frac{\partial\psi_x}{\partial y}\right)\right) \tag{A.2}$$

$$\tau_{xz} = \hat{\mu}\left(2\frac{\partial^2\varphi}{\partial x\partial z} + \frac{\partial}{\partial z}\left(\frac{\partial\psi_z}{\partial y} - \frac{\partial\psi_y}{\partial z}\right) + \frac{\partial}{\partial x}\left(\frac{\partial\psi_y}{\partial x} - \frac{\partial\psi_x}{\partial y}\right)\right) \tag{A.3}$$

$$\tau_{yz} = \hat{\mu}\left(2\frac{\partial^2\varphi}{\partial y\partial z} - \frac{\partial}{\partial z}\left(\frac{\partial\psi_z}{\partial x} - \frac{\partial\psi_x}{\partial z}\right) + \frac{\partial}{\partial y}\left(\frac{\partial\psi_y}{\partial x} - \frac{\partial\psi_x}{\partial y}\right)\right) \tag{A.4}$$

Appendix B

The matrix $[\boldsymbol{C}]$ and vector $\boldsymbol{F}$ in Eq. (16) are given as

$$[\boldsymbol{C}] = \begin{bmatrix} 0 & 0 & \mathrm{i}k_1 & 0 & \mathrm{i}k_2 & 0 & R_\mathrm{T} & 0 \\ 0 & 0 & 0 & \mathrm{i}k_1 & 0 & \mathrm{i}k_2 & 0 & -R_\mathrm{T} \\ \mathrm{i}k_1a_1 & \mathrm{i}k_1/a_1 & 0 & 0 & -R_\mathrm{T}b_1 & R_\mathrm{T}/b_1 & \mathrm{i}k_2b_1 & \mathrm{i}k_2/b_1 \\ \mathrm{i}k_2a_1 & \mathrm{i}k_2/a_1 & R_\mathrm{T}b_1 & -R_\mathrm{T}/b_1 & 0 & 0 & -\mathrm{i}k_1b_1 & -\mathrm{i}k_1/b_1 \\ R_\mathrm{L}a_1 & -R_\mathrm{L}/a_1 & -\mathrm{i}k_2b_1 & \mathrm{i}k_2/b_1 & \mathrm{i}k_1b_1 & \mathrm{i}k_1/b_1 & 0 & 0 \\ 2\mathrm{i}k_1R_\mathrm{L} & -2\mathrm{i}k_1R_\mathrm{L} & k_1k_2 & k_1k_2 & -(R_\mathrm{T}^2+k_1^2) & -(R_\mathrm{T}^2+k_1^2) & \mathrm{i}k_2R_\mathrm{T} & -\mathrm{i}k_2R_\mathrm{T} \\ 2\mathrm{i}k_2R_\mathrm{L} & -2\mathrm{i}k_2R_\mathrm{L} & R_\mathrm{T}^2+k_2^2 & R_\mathrm{T}^2+k_2^2 & -k_1k_2 & -k_1k_2 & -\mathrm{i}k_1R_\mathrm{T} & \mathrm{i}k_1R_\mathrm{T} \\ \gamma & \gamma & -2\mathrm{i}k_2R_\mathrm{T} & 2\mathrm{i}k_2R_\mathrm{T} & 2\mathrm{i}k_1R_\mathrm{T} & -2\mathrm{i}k_1R_\mathrm{T} & 0 & 0 \end{bmatrix} \tag{B.1}$$

$$F = \{0,0,0,0,0,F_1,0,F_3\} \tag{B.2}$$

with

$$
\begin{aligned}
a_1 &= \exp(R_{\mathrm{L}}H), \quad b_1 = \exp(R_{\mathrm{T}}H), \quad \gamma = 2R_{\mathrm{T}}^2 + \omega^2/\tilde{c}_{\mathrm{T}}^2,\\
F_1 &= \frac{1}{\tilde{\mu}}\frac{\sin k_1 b}{k_1 b}\frac{\sin k_2 a}{k_2 a}\sum_{n=-\infty}^{\infty} Ku_{\omega}(nd,0,0,\omega)\exp(-\mathrm{i}k_1 nd),\\
F_3 &= \frac{1}{\tilde{\mu}}\frac{\sin k_1 b}{k_1 b}\frac{\sin k_2 a}{k_2 a}\sum_{n=-\infty}^{\infty}[-M\omega^2 W_{\omega}^{n}(\omega) + 2(K_{\mathrm{p}} - \mathrm{i}\varepsilon_{\mathrm{p}})(w_{\omega}(nd,0,0,\omega)\\
&\quad - w_{\omega}^{\mathrm{beam}}(nd,\omega))]\exp(-\mathrm{i}k_1 nd)
\end{aligned}
\tag{B.3}
$$

Expressions for a_{11}, a_{13}, a_{31} and a_{33} in Eq. (17) read

$$
\begin{aligned}
a_{11} &= \frac{1}{\Delta}\{-k_2^2 R_{\mathrm{L}}R_{\mathrm{T}}\sinh R_{\mathrm{T}}H((4(k_1^2+k_2^2)+\gamma)\cosh R_{\mathrm{L}}H\cosh R_{\mathrm{T}}H - 2(\gamma+k_1^2+k_2^2))\\
&\quad + R_{\mathrm{T}}^2\sinh R_{\mathrm{L}}H(k_2^2(\gamma+4R_{\mathrm{L}}^2)\sinh^2 R_{\mathrm{T}}H + k_1^2(\gamma-2(k_1^2+k_2^2))\cosh^2 R_{\mathrm{T}}H)\\
&\quad + R_{\mathrm{L}}R_{\mathrm{T}}^3\sinh R_{\mathrm{T}}H((2k_1^2-\gamma)\cosh R_{\mathrm{L}}H\cosh R_{\mathrm{T}}H + 2k_2^2) + \gamma k_2^2(k_1^2+k_2^2)\sinh R_{\mathrm{L}}H\sinh^2 R_{\mathrm{T}}H\}\\
a_{13} &= k_1 a_{13}^0,\\
a_{13}^0 &= \frac{\mathrm{i}R_{\mathrm{T}}}{\Delta}\cosh R_{\mathrm{T}}H\{\gamma(k_1^2+k_2^2)\sinh R_{\mathrm{L}}H\sinh R_{\mathrm{T}}H\\
&\quad + R_{\mathrm{L}}R_{\mathrm{T}}(2R_{\mathrm{L}}R_{\mathrm{T}}\sinh R_{\mathrm{L}}H\sinh R_{\mathrm{T}}H + (\gamma+2(k_1^2+k_2^2))(1-\cosh R_L H\cosh R_{\mathrm{T}}H))\},\\
a_{33} &= \cosh R_{\mathrm{T}}H\frac{R_{\mathrm{L}}R_{\mathrm{T}}}{\Delta}\frac{\omega^2}{\tilde{c}_{\mathrm{T}}^2}\{R_{\mathrm{L}}R_{\mathrm{T}}\sinh R_{\mathrm{L}}H\cosh R_{\mathrm{T}}H - (k_1^2+k_2^2)\cosh R_{\mathrm{L}}H\sinh R_{\mathrm{T}}H\},\\
a_{31} &= -a_{13},\\
\Delta &= R_{\mathrm{T}}\cosh R_{\mathrm{T}}H\{R_{\mathrm{L}}R_{\mathrm{T}}(4(k_1^2+k_2^2)^2+\gamma^2)\cosh R_{\mathrm{L}}H\cosh R_{\mathrm{T}}H\\
&\quad - (k_1^2+k_2^2)((4R_{\mathrm{L}}^2R_{\mathrm{T}}^2+\gamma^2)\sinh R_{\mathrm{L}}H\sinh R_{\mathrm{T}}H + 4R_{\mathrm{L}}R_{\mathrm{T}}\gamma)\} = \Delta_0 R_{\mathrm{T}}\cosh R_{\mathrm{T}}H
\end{aligned}
\tag{B.4}
$$

Appendix C

To evaluate Eq. (29), we rewrite it in the following form

$$
J_{kj} = \frac{1}{4\pi^2\tilde{\mu}}\frac{1}{2\mathrm{i}ab}\int_{-\infty}^{\infty}\frac{\sin k_2 a}{k_2}S_{kj}^0(k_2,\omega)\,\mathrm{d}k_2, \quad k=1,3;\ \ j=1,3, \tag{C.1}
$$

where

$$
S_{kj}^0(k_2,\omega) = \sum_{n=-\infty}^{\infty}\exp(-\mathrm{i}qn)\int_{-\infty}^{\infty}a_{kj}\frac{\mathrm{e}^{\mathrm{i}k_1(dn+b)} - \mathrm{e}^{\mathrm{i}k_1(dn-b)}}{k_1}\,\mathrm{d}k_1. \tag{C.2}
$$

Let us first deal with the integral in Eq. (C.2), the integrand of which consists of two terms that are proportional to $\exp(\mathrm{i}k_1(dn+b))$ and $\exp(\mathrm{i}k_1(dn-b))$. Both terms can be evaluated simultaneously considering the following integral

$$
Z_{kj}(r) = \int_{-\infty}^{\infty}a_{kj}(k_1,k_2,\omega)\frac{\mathrm{e}^{\mathrm{i}k_1 r}}{k_1}\,\mathrm{d}k_1, \quad r = nd \pm b. \tag{C.3}
$$

Integration of Eq. (C.3) will be performed using the method of contour integration (Fuchs et al., 1964). To apply this method, singular points of the integrand should be determined. The integrand in Eq. (C.3) are

single-valued functions despite the radicals R_{L} and R_{T}. These radicals do not make the integrand multi-valued since the replacement $R_{\mathrm{L,T}} \to -R_{\mathrm{L,T}}$ does not change the integrand. Thus, only poles of the integrand should be considered. All these poles are simple and defined by the following equations

for Z_{33}

$$\Delta_0 = 0, \quad k_1 = 0, \tag{C.4}$$

for Z_{13}

$$\Delta_0 = 0, \tag{C.5}$$

for Z_{11}

$$\Delta_0 = 0, \quad \cosh R_{\mathrm{T}} H = 0, \quad k_1 = 0, \tag{C.6}$$

with (see also (B.4))

$$\begin{aligned}\Delta_0 = {} & R_{\mathrm{L}} R_{\mathrm{T}} (4(k_1^2 + k_2^2)^2 + \gamma^2) \cosh R_{\mathrm{L}} H \cosh R_{\mathrm{T}} H \\ & - (k_1^2 + k_2^2)((4R_{\mathrm{L}}^2 R_{\mathrm{T}}^2 + \gamma^2) \sinh R_{\mathrm{L}} H \sinh R_{\mathrm{T}} H + 4R_{\mathrm{L}} R_{\mathrm{T}} \gamma).\end{aligned} \tag{C.7}$$

Having defined (though implicitly) positions of the poles in the complex k_1-plane, we have to close the original integration path that runs from minus to plus infinity along the real axis. This can be done with the help of a semi-circle (with its center at the origin) that is positioned either in the upper or lower half-plane of the complex k_1-plane. Which half-plane is to be chosen is dictated by Jordan's lemma (Abramowitz and Stegun, 1970), which ensures that the integration along the chosen semi-circle vanishes as its radius tends to infinity. In application to Eq. (C.3), the path has to be closed over the upper half-plane if $r > 0$ (see Fig. 12) and over the lower half-plane if $r < 0$.

Now the residue theorem can be applied, according to which an integral along a closed contour can be expressed through the sum of residues over poles that are located within this contour. In our case this theorem yields

for $r > 0$

$$\begin{aligned}\oint a_{11}(k_1, k_2, \omega) \frac{\mathrm{e}^{\mathrm{i}k_1 r}}{k_1} \mathrm{d}k_1 &= Z_{11}(r) - \pi \mathrm{i} a_{11}(0, k_2, \omega) = 2\pi \mathrm{i} \sum_m \operatorname{res}\left\{ a_{11}(k_1, k_2, \omega) \frac{\mathrm{e}^{\mathrm{i}k_1 r}}{k_1} \right\}_{k_1 = k_1^m}, \\ \oint a_{33}(k_1, k_2, \omega) \frac{\mathrm{e}^{\mathrm{i}k_1 r}}{k_1} \mathrm{d}k_1 &= Z_{33}(r) - \pi \mathrm{i} a_{33}(0, k_2, \omega) = 2\pi \mathrm{i} \sum_m \operatorname{res}\left\{ a_{33}(k_1, k_2, \omega) \frac{\mathrm{e}^{\mathrm{i}k_1 r}}{k_1} \right\}_{k_1 = k_1^m}, \\ \oint a_{13}(k_1, k_2, \omega) \frac{\mathrm{e}^{\mathrm{i}k_1 r}}{k_1} \mathrm{d}k_1 &= Z_{13}(r) = 2\pi \mathrm{i} \sum_m \operatorname{res}\{ a_{13}^0(k_1, k_2, \omega) \mathrm{e}^{\mathrm{i}k_1 r} \}_{k_1 = k_1^m},\end{aligned} \tag{C.8}$$

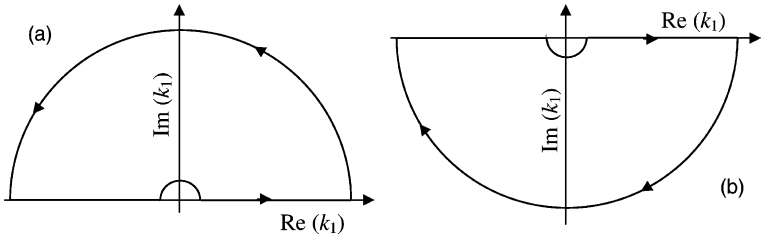

Fig. 12. Integration contour for (a) $r > 0$ and (b) $r < 0$.

for $r < 0$

$$\begin{aligned}
\oint a_{11}(k_1,k_2,\omega)\frac{e^{ik_1 r}}{k_1}dk_1 &= Z_{11}(r) + \pi i a_{11}(0,k_2,\omega) = -2\pi i \sum_l \operatorname{res}\left\{ a_{11}(k_1,k_2,\omega)\frac{e^{ik_1 r}}{k_1}\right\}_{k_1=k_1^l},\\
\oint a_{33}(k_1,k_2,\omega)\frac{e^{ik_1 r}}{k_1}dk_1 &= Z_{33}(r) + \pi i a_{33}(0,k_2,\omega) = -2\pi i \sum_l \operatorname{res}\left\{ a_{33}(k_1,k_2,\omega)\frac{e^{ik_1 r}}{k_1}\right\}_{k_1=k_1^l},\\
\oint a_{13}(k_1,k_2,\omega)\frac{e^{ik_1 r}}{k_1}dk_1 &= Z_{13}(r) = -2\pi i \sum_l \operatorname{res}\{a_{13}^0(k_1,k_2,\omega)e^{ik_1 r}\}_{k_1=k_1^l},
\end{aligned} \tag{C.9}$$

with k_1^m and k_1^l the roots defined by Eqs. (C.4)–(C.6) located in the upper half-plane and the lower half-plane of the complex k_1-plane, respectively ($\mathrm{Im}(k_1^m) > 0, \mathrm{Im}(k_1^l) < 0$).

Expressing $Z_{ij}(r)$ from Eqs. (C.8) and (C.9), we obtain

for $r > 0$

$$\begin{aligned}
Z_{11}(r) &= \pi i a_{11}(0,k_2,\omega) + 2\pi i \sum_m \operatorname{res}\left\{ a_{11}(k_1,k_2,\omega)\frac{e^{ik_1 r}}{k_1}\right\}_{k_1=k_1^m},\\
Z_{33}(r) &= \pi i a_{33}(0,k_2,\omega) + 2\pi i \sum_m \operatorname{res}\left\{ a_{33}(k_1,k_2,\omega)\frac{e^{ik_1 r}}{k_1}\right\}_{k_1=k_1^m},\\
Z_{13}(r) &= 2\pi i \sum_m \operatorname{res}\{a_{13}^0(k_1,k_2,\omega)e^{ik_1 r}\}_{k_1=k_1^m},
\end{aligned} \tag{C.10}$$

for $r < 0$

$$\begin{aligned}
Z_{11}(r) &= -\pi i a_{11}(0,k_2,\omega) - 2\pi i \sum_l \operatorname{res}\left\{ a_{11}(k_1,k_2,\omega)\frac{e^{ik_1 r}}{k_1}\right\}_{k_1=k_1^l},\\
Z_{33}(r) &= -\pi i a_{33}(0,k_2,\omega) - 2\pi i \sum_l \operatorname{res}\left\{ a_{33}(k_1,k_2,\omega)\frac{e^{ik_1 r}}{k_1}\right\}_{k_1=k_1^l},\\
Z_{13}(r) &= -2\pi i \sum_l \operatorname{res}\{a_{13}^0(k_1,k_2,\omega)e^{ik_1 r}\}_{k_1=k_1^l}.
\end{aligned} \tag{C.11}$$

Now that expressions for $Z_{kj}(r)$ have been found, we can return to Eq. (C.2) for $S_{kj}^0(k_2,\omega)$, which can be expressed through $Z_{kj}(r)$ in the following manner

$$\begin{aligned}
S_{kj}^0(k_2,\omega) &= \sum_{n=-\infty}^{\infty} \exp(-iqn)(Z_{kj}(nd+b) - Z_{kj}(nd-b))\\
&= Z_{kj}(b) - Z_{kj}(-b) + \sum_{n=1}^{\infty} e^{-iqn}(Z_{kj}(nd+b) - Z_{kj}(nd-b))\\
&\quad + \sum_{n=1}^{\infty} e^{iqn}(Z_{kj}(-nd+b) - Z_{kj}(-nd-b)).
\end{aligned} \tag{C.12}$$

Since the distance between the neighboring sleepers d is always larger than the longitudinal size of the sleepers $2b$, it is obvious that for $n \geqslant 1$, $nd \pm b > 0$ and $-nd \pm b < 0$. This implies that to evaluate $Z_{kj}(nd \pm b)$ we have to use expressions (C.10) ($r > 0$), whilst to evaluate $Z_{kj}(-nd \pm b)$ expressions (C.11) ($r < 0$) have to be used.

Eq. (12) can be simplified by using symmetry properties of the functions $Z_{kj}(r)$. These properties read

$$\begin{aligned} Z_{11}(r) &= -Z_{11}(-r), \\ Z_{33}(r) &= -Z_{33}(-r), \\ Z_{13}(r) &= Z_{13}(-r) \end{aligned} \tag{C.13}$$

and follow from the following symmetry properties of the functions a_{11}, a_{33} and a_{13}

$$\begin{aligned} a_{11}(k_1,k_2,\omega) &= a_{11}(-k_1,k_2,\omega), \\ a_{33}(k_1,k_2,\omega) &= a_{33}(-k_1,k_2,\omega), \\ a^0_{13}(k_1,k_2,\omega) &= a^0_{13}(-k_1,k_2,\omega), \end{aligned} \tag{C.14}$$

which implies that

$$\begin{aligned} &2\pi\mathrm{i}\sum_m \mathrm{res}\left\{a_{jj}(k_1,k_2,\omega)\frac{\mathrm{e}^{\mathrm{i}k_1 r}}{k_1}\right\}_{k_1=k_1^m} = 2\pi\mathrm{i}\sum_l \mathrm{res}\left\{a_{jj}(k_1,k_2,\omega)\frac{\mathrm{e}^{\mathrm{i}k_1 r}}{k_1}\right\}_{k_1=k_1^l}, \quad j=1,3 \\ &2\pi\mathrm{i}\sum_m \mathrm{res}\{a^0_{13}(k_1,k_2,\omega)\mathrm{e}^{\mathrm{i}k_1 r}\}_{k_1=k_1^m} = -2\pi\mathrm{i}\sum_l \mathrm{res}\{a^0_{13}(k_1,k_2,\omega)\mathrm{e}^{\mathrm{i}k_1 r}\}_{k_1=k_1^l}. \end{aligned} \tag{C.15}$$

Employing relationships (C.13), Eq. (12) is reduced to

$$\begin{aligned} S^0_{jj}(k_2,\omega) &= 2Z_{jj}(b) + \sum_{n=1}^{\infty}(\mathrm{e}^{\mathrm{i}nq}+\mathrm{e}^{-\mathrm{i}nq})(\widetilde{Z}_{jj}(nd+b)-\widetilde{Z}_{jj}(nd-b)), \quad j=1,3 \\ S^0_{13}(k_2,\omega) &= \sum_{n=1}^{\infty}(\mathrm{e}^{-\mathrm{i}nq}-\mathrm{e}^{\mathrm{i}nq})(Z_{13}(nd+b)-Z_{13}(nd-b)), \end{aligned} \tag{C.16}$$

where

$$\widetilde{Z}_{jj}(r) = 2\pi\mathrm{i}\sum_m \mathrm{res}\left\{a_{jj}(k_1,k_2,\omega)\frac{\mathrm{e}^{\mathrm{i}k_1 r}}{k_1}\right\}_{k_1=k_1^m}, \quad j=1,3. \tag{C.17}$$

To obtain expressions (C.16), we used the following chain of equalities

$$\begin{aligned} Z_{jj}(nd+b)-Z_{jj}(nd-b) &= 2\pi\mathrm{i}\sum_m \mathrm{res}\left\{a_{jj}(k_1,k_2,\omega)\frac{\mathrm{e}^{\mathrm{i}k_1 r}}{k_1}\right\}_{\substack{k_1=k_1^m,\\ r=nd+b}} + \pi\mathrm{i}a_{jj}(0,k_2,\omega) \\ &\quad - \left(2\pi\mathrm{i}\sum_m \mathrm{res}\left\{a_{jj}(k_1,k_2,\omega)\frac{\mathrm{e}^{\mathrm{i}k_1 r}}{k_1}\right\}_{\substack{k_1=k_1^m,\\ r=nd-b}} + \pi\mathrm{i}a_{jj}(0,k_2,\omega)\right) \\ &= 2\pi\mathrm{i}\sum_m \mathrm{res}\left\{a_{jj}(k_1,k_2,\omega)\frac{\mathrm{e}^{\mathrm{i}k_1 r}}{k_1}\right\}_{\substack{k_1=k_1^m,\\ r=nd+b}} - 2\pi\mathrm{i}\sum_m \mathrm{res}\left\{a_{jj}(k_1,k_2,\omega)\frac{\mathrm{e}^{\mathrm{i}k_1 r}}{k_1}\right\}_{\substack{k_1=k_1^m,\\ r=nd-b}} \\ &= \widetilde{Z}_{jj}(nd+b)-\widetilde{Z}_{jj}(nd-b). \end{aligned} \tag{C.18}$$

Further simplification of Eq. (C.16) can be carried out by analytically calculating the infinite series with respect to n. Let us show the way to do this on the hand of the following term (for all other terms, this can be done in exactly the same manner)

$$Q = \sum_{n=1}^{\infty}\mathrm{e}^{\mathrm{i}nq}\widetilde{Z}_{jj}(nd+b). \tag{C.19}$$

Substituting expression for $\widetilde{Z}_{jj}$ given by Eq. (C.17) into Eq. (C.19) equation, we obtain

$$Q = 2\pi \mathrm{i} \sum_{n=1}^{\infty} \mathrm{e}^{\mathrm{i}nq} \sum_{m} \operatorname{res}\left\{ a_{jj}(k_1, k_2, \omega) \frac{\mathrm{e}^{\mathrm{i}k_1 r}}{k_1} \right\}_{k_1 = k_1^m}. \tag{C.20}$$

Introducing the notation $k_1^m = k'_m + \mathrm{i}k''_m$ with k'_m and k''_m real values and $k''_m > 0$ (by definition, see Eq. (C.8)), and changing the order of summation, Eq. (C.20) can be rewritten as

$$\begin{aligned} Q &= 2\pi \mathrm{i} \sum_{n=1}^{\infty} \mathrm{e}^{\mathrm{i}nq} \sum_{m} \operatorname{res}\left\{ a_{jj}(k_1, k_2, \omega) \frac{\mathrm{e}^{\mathrm{i}k_1(nd+b)}}{k_1} \right\}_{k_1 = k_1^m} \\ &= 2\pi \mathrm{i} \sum_{m} \mathrm{e}^{\mathrm{i}b(k'_m + \mathrm{i}k''_m)} \operatorname{res}\left\{ \frac{a_{jj}(k_1, k_2, \omega)}{k_1} \right\}_{k_1 = k_1^m} \sum_{n=1}^{\infty} \mathrm{e}^{\mathrm{i}n}(q + dk'_m) - ndk''_m. \end{aligned} \tag{C.21}$$

The series over n in Eq. (C.21) is geometric progression with infinite number of terms and the common ratio of successive terms $p = \mathrm{e}^{\pm \mathrm{i}nq} \mathrm{e}^{\mathrm{i}k'_m nd} \mathrm{e}^{-k''_m nd}$, $|p| < 1$.

Using the following formula for the sum of infinite geometric progression

$$\sum_{n=1}^{\infty} p^n = \frac{p}{1-p}. \tag{C.22}$$

Eq. (C.21) can be rewritten as

$$\begin{aligned} Q &= 2\pi \mathrm{i} \sum_{m} \mathrm{e}^{\mathrm{i}b(k'_m + \mathrm{i}k''_m)} \operatorname{res}\left\{ \frac{a_{jj}(k_1, k_2, \omega)}{k_1} \right\}_{k_1 = k_1^m} \sum_{n=1}^{\infty} \mathrm{e}^{\mathrm{i}n}(q + dk'_m) - ndk''_m \\ &= 2\pi \mathrm{i} \sum_{m} \mathrm{e}^{\mathrm{i}b(k'_m + \mathrm{i}k''_m)} \operatorname{res}\left\{ \frac{a_{jj}(k_1, k_2, \omega)}{k_1} \right\}_{k_1 = k_1^m} \frac{\exp(\mathrm{i}(q + dk'_m) - dk''_m)}{1 - \exp(\mathrm{i}d(q + k'_m) - dk''_m)} \\ &= 2\pi \mathrm{i} \sum_{m} \mathrm{e}^{\mathrm{i}bk_1^m} \operatorname{res}\left\{ \frac{a_{jj}(k_1, k_2, \omega)}{k_1} \right\}_{k_1 = k_1^m} \frac{\exp(\mathrm{i}k_1^m d \pm \mathrm{i}q)}{1 - \exp(\mathrm{i}k_1^m d \pm \mathrm{i}q)}. \end{aligned} \tag{C.23}$$

Evaluating the series over n in the other terms of Eq. (C.16), this equation can be reduced to the following form

$$\begin{aligned} S_{jj}^0(k_2, \omega) = 2\pi \mathrm{i} a_{jj}(0, k_2, \omega) + 2\pi \mathrm{i} \sum_{m=1}^{\infty} \operatorname{res}\left\{ \frac{a_{jj}(k_1, k_2, \omega)}{k_1} \right\}_{k_1 = k_1^m} \\ \times \left[2\mathrm{e}^{\mathrm{i}k_1^m b} + (\mathrm{e}^{\mathrm{i}k_1^m b} - \mathrm{e}^{-\mathrm{i}k_1^m b}) \left\{ \frac{\exp(\mathrm{i}k_1^m d + \mathrm{i}q)}{1 - \exp(\mathrm{i}k_1^m d + \mathrm{i}q)} + \frac{\exp(\mathrm{i}k_1^m d - \mathrm{i}q)}{1 - \exp(\mathrm{i}k_1^m d - \mathrm{i}q)} \right\} \right] \end{aligned} \tag{C.24}$$

$$S_{13}^0(k_2, \omega) = 2\pi \mathrm{i} \sum_{m=1}^{\infty} \operatorname{res}\{a_{13}^0(k_1, k_2, \omega)\}_{k_1 = k_1^m} (\mathrm{e}^{\mathrm{i}k_1^m b} - \mathrm{e}^{-\mathrm{i}k_1^m b}) \left\{ \frac{\exp(\mathrm{i}k_1^m d - \mathrm{i}q)}{1 - \exp(\mathrm{i}k_1^m d - \mathrm{i}q)} - \frac{\exp(\mathrm{i}k_1^m d + \mathrm{i}q)}{1 - \exp(\mathrm{i}k_1^m d + \mathrm{i}q)} \right\} \tag{C.25}$$

Substituting Eqs. (C.24) and (C.25) into Eq. (C.1), and carrying out regular algebraic manipulations, expressions for the coefficients J_{kj} can be obtained that are given by Eq. (30).

Appendix D

Substitution of Eqs. (47) and (49) into the boundary conditions (44) and (45) gives the following system of equations

$$
\begin{aligned}
&C_1\exp(\alpha d)+C_2\exp(-\alpha d)+C_3\exp(\mathrm{i}\alpha d)+C_4\exp(-\mathrm{i}\alpha d)=q_0(C_1+C_2+C_3+C_4),\\
&C_1\exp(\alpha d)-C_2\exp(-\alpha d)+\mathrm{i}C_3\exp(\mathrm{i}\alpha d)-\mathrm{i}C_4\exp(-\mathrm{i}\alpha d)=q_0(C_1-C_2+\mathrm{i}C_3-\mathrm{i}C_4),\\
&C_1\exp(\alpha d)+C_2\exp(-\alpha d)-C_3\exp(\mathrm{i}\alpha d)-C_4\exp(-\mathrm{i}\alpha d)=q_0(C_1+C_2-C_3-C_4),\\
&EI\alpha^3q_0(C_1-C_2-\mathrm{i}C_3+\mathrm{i}C_4)-EI\alpha^3(C_1\exp(\alpha d)-C_2\exp(-\alpha d)\\
&\quad-\mathrm{i}C_3\exp(\mathrm{i}\alpha d)+\mathrm{i}C_4\exp(-\mathrm{i}\alpha d))=-C_0(K_\mathrm{p}-\mathrm{i}\omega\varepsilon_\mathrm{p})B_0(\omega)q_0,\\
&C_1+C_2+C_3+C_4-F_0=C_0,
\end{aligned}
\tag{D.1}
$$

with $q=\exp(\mathrm{i}d(\omega+\Omega)/V)$.

When solved for C_j $(j=1,\ldots,4)$ this system gives

$$
\begin{aligned}
&C_j=\Delta_j/\Delta,\quad j=1,\ldots,4\\
&\Delta=4\mathrm{i}q_0\left\{4EJ\alpha^3B_0/(T_0(B_0-T_0))\left(\cos\frac{\omega d}{V}-\cosh\alpha d\right)\left(\cos\frac{\omega d}{V}-\cos\alpha d\right)\right.\\
&\qquad\left.+\left(\cos\frac{\omega d}{V}(\sinh\alpha d-\sin\alpha d)+\cosh\alpha d\sin\alpha d-\sinh\alpha d\cos\alpha d\right)\right\}\\
&\Delta_1=\mathrm{i}F_0\{q_0^3-q_0^2(\exp(-\alpha d)+2\cos(\alpha d))+q_0(1+2\exp(-\alpha d)\cos(\alpha d))-\exp(-\alpha d)\},\\
&\Delta_2=-\mathrm{i}F_0\{q_0^3-q_0^2(\exp(\alpha d)+2\cos(\alpha d))+q_0(1+2\exp(\alpha d)\cos(\alpha d))-\exp(\alpha d)\},\\
&\Delta_3=-F_0\{q_0^3-q_0^2(\exp(-\mathrm{i}\alpha d)+2\cosh(\alpha d))+q_0(1+2\exp(-\mathrm{i}\alpha d)\cosh(\alpha d))-\exp(-\mathrm{i}\alpha d)\},\\
&\Delta_4=F_0\{q_0^3-q_0^2(\exp(\mathrm{i}\alpha d)+2\cosh(\alpha d))+q_0(1+2\exp(\mathrm{i}\alpha d)\cosh(\alpha d))-\exp(\mathrm{i}\alpha d)\},\\
&T_0=K_\mathrm{p}-\mathrm{i}\omega\varepsilon_\mathrm{p}.
\end{aligned}
\tag{D.2}
$$

References

Abramowitz, M., Stegun, I.A., 1970. Handbook of Mathematical Functions: with Formulas, Graphs, and Mathematical Tables. Dover, New York.

Achenbach, J.D., 1973. Wave Propagation in Elastic Solids. NHPC, Amsterdam, London.

Belotserkovskiy, P.M., 1996. On the oscillations of infinite periodic beams subjected to a moving concentrated force. Journal of Sound and Vibration 193 (3), 706–712.

Dieterman, H.A., Metrikine, A.V., 1996. The equivalent stiffness of a half-space interacting with a beam. Critical velocities of a moving load along the beam. European Journal of Mechanics A/Solids 15 (1), 67–90.

Filippov, A.P., 1961. Steady-state vibrations of a infinite beam on an elastic half-space under moving load. Izvestija AN SSSR OTN Mehanica and Mashinostroenie 6, 97–105.

Fuchs, B.A., Shabat, B.V., Berry, J., 1964. Functions of a Complex Variable and Some of their Applications. Pergamon, Oxford.

Grundmann, H., Lieb, M., Trommer, E., 1999. The response of a layered half-space to traffic loads moving along its surface. Archive of Applied Mechanics 69 (1), 55–67.

Hopkins, T., Silva, J.P., Marder, B., Turban, B., Kelley, B., 1999. Maglift Monorail: a high performance, low cost, and low risk solution for high-speed transportation. In: Proceedings of High Speed Ground Transportation Association. Annual Conference, Seatle.

Kausel, E., Roësset, J.M., 1981. Stiffness matrices for layered soils. Bulletin of the Seismological Society of America 71, 1743–1761.

Kaynia, A.M., Madhus, C., Zackrisson, P., 2000. Ground vibration from high-speed trains: prediction and countermeasure. Journal of Geotechnical Geoenvironmental Engineering 126 (6), 531–537.

Krylov, V.V., 1995. Generation of ground vibrations by superfast trains. Applied Acoustics 44 (2), 149–164.

Labra, J.J., 1975. An axially stressed railroad track on an elastic continuum subjected to a moving load. Acta Mechanica 22, 113–129.

Metrikine, A.V., Dieterman, H.A., 1997. Three-dimensional vibrations of a beam on an elastic half-space: resonance interaction of vertical-longitudinal and lateral beam waves. Transactions of ASME Journal of Applied Mechanics 64, 951–956.

Metrikine, A.V., Popp, K., 1999. Vibration of a periodically supported beam on an elastic half-space. European Journal of Mechanics A/Solids 18 (4), 679–701.

Metrikine, A.V., Vostrukhov, A.V., Vrouwenvelder, A.C.W.M., 2001. Drag experienced by a high-speed train due to excitation of ground vibrations. International Journal of Solid and Structures 38, 8851–8868.

Sheng, X., Jones, C.J.C., Petyt, M., 1999. Ground vibration generated by a load moving along a railway track. Journal of Sound and Vibration 228 (1), 129–156.

Van den Broeck, P., Degrande, G., De Roeck, G., 2002. A prediction model for ground-borne vibrations due to railway traffic. In: Grundmann, H., Schuëller, G.I. (Eds.), EURODYN2002, Munich, Germany. pp. 503–508.

Vesnitskii, A.I., Metrikine, A.V., 1996. Transition radiation in mechanics. Physics–Uspekhi 39 (10), 983–1007.

Vladimirov, V.S., 1979. Generalized functions in mathematical physics author, Moscow, Mir.